UNIVERSITY OF OSLO
Department of Physics

Natural circulating flat plate collectors

Investigations of a new material and performance simulations

Master's thesis in Physics, Teacher Education Programme

Aylin Maria Dursun

May 27th, 2013

Abstract

Solar energy can be utilized to heat water with the use of flat plate collectors. Effort is made to reduce the cost of solar water heating technology in order to make it economically competitive to conventional energy. An absorber material is tested on component level and performance related aspects are studied. The material has a lower price than the polymer materials currently used in glazed collectors, and therefore it has the potential to lower the cost of solar flat plate collectors. The performance related aspects are tested on a partially glazed, natural circulating flat plate collector, referred to as the Duo-Collector. The aim of letting the collector be partially glazed is to prevent the heat carrier from boiling. Samples cut from an extruded absorber sheet were exposed to 140 °C and 150 °C for different periods of time. These were used to map the mechanical properties of the material. The samples exposed to 150 °C were used to map dimensional and optical changes. The results from the material-related studies on component level show that no failure occurs for any of the ageing periods which were realized in the time frame of the present work. The extruded absorber sheet has a sufficiently high absorptance and dimensional stability. These findings have strengthened the material's position as a candidate for use in solar thermal applications. The performance of the Duo-Collector has been simulated with MATLAB®. It is found that the system is suitable as a method for preventing the fluid in the collector from boiling. The efficiency of such a system was also investigated. For low operating temperatures the efficiency of a Duo-Collector is approximately equal to the efficiency of a fully glazed or an unglazed collector. The efficiency of all the collectors decrease with increasing operating temperatures, and the efficiency of the Duo-Collector is between that of a fully glazed and that of an unglazed collector for all operating temperatures above approximately 10 °C. Under certain circumstances the Duo-Collector can cool the water. This effect needs to be investigated further. Since only steady-state conditions are studied in this work, further analysis must be performed to compare how the Duo-Collector performs for different applications.

Acknowledgements

I am deeply grateful to Professor John Rekstad and Dr. Michaela Meir for giving me the opportunity to write this master´s thesis and for always being positive, flexible and supporting. It has been a great experience to work with you.

The last eighteen weeks have given me a large variety of challenges, and I am thankful to all the people who have made the process a little easier; thanks to all the friendly people at SAFE, thank you Dag for lending me a heating cabinet, thanks to the people doing IT support and to the guys at the workshop. Thank you Professor John Grue for your interest and help when I showed up in your office.

Thank you for your friendship Inger Helene and Ida.

My lovely family has always been a great support. Thank you for your unconditional love and your second opinion.

Aylin Dursun

Contents

1 Introduction **1**

2 Solar heating systems **5**
2.1 Studies on low cost systems 5
2.2 Flat plate collectors 7
2.3 Thermosyphon systems 9
2.4 Heat carrier temperature 10
2.5 The Duo-Collector 11

3 Polymer science **15**
3.1 Polypropylene 15
3.2 Elasticity and plasticity 15
3.3 Ageing 17
3.4 Mathematical model of degradation 18
3.5 Service life estimations 19

4 Experimental setup **21**
4.1 The alphameter 21
4.2 The Instron 3345 machine 21
4.3 Termaks heating cabinets 22
4.4 Absorber material and design 22

5 Experimental studies **25**
5.1 Approach 25
5.2 Results 30

6 Simulation **33**
6.1 Approach 33
6.2 Results 40

7 Discussion **45**
7.1 Discussion of experimental results 45
7.2 Discussion of results from simulation 49

8 Summary **53**

Bibliography **55**

Appendices **59**

A Results from earlier studies **61**

B MATLAB scripts **65**

C Indentation tests **69**

D Raw data: dimensions **71**

E Raw data: absorptance **73**

Nomenclature

A	collector area [m^2]
A_c	cross section area [m^2]
b	plate thickness [m]
c	specific heat capacity [J/(kgK)]
C	proportionality constant
C_1	constant of integration
D	thermal dose
D_c	critical thermal dose
$\mathrm{d}x$	aperture between inner walls [m]
$\mathrm{d}z$	aperture between plates [m]
E_a	activation energy
F	force needed to bring specimen to fracture point
F_0	force needed to bring unexposed specimen to fracture point
F_c	critical load
F'	collector efficiency factor
g	acceleration due to gravity [m/s^2]
G	solar irradiance incident on collector surface [W/m^2]
h	height of absorber [m]
h_1	height of glazed part of absorber [m]
h_2	height of unglazed part of absorber [m]
H	defined as k_p/b [$W/(m^2K)$]
k	the Boltzmann constant
k_1	loss coefficient to be fitted experimentally [W/m^2K]
k_2	loss coefficient to be fitted experimentally [W/m^2K^2]
k_p	thermal conductivity of plate [W/(mK)]
m	mass
n	reaction order
P	glazing fraction [%]
P_0	ambient pressure [Pa]
P_1	pressure at the bottom of water column [Pa]
q_u	unit area useful energy rate [W/m^2]
Q_u	useful energy rate [W]
S	absorbed solar radiation [W/m^2]
t	time [s]
T	temperature [°C]
T_a	ambient temperature [°C]
T_d	temperature difference between heat carrier and ambient
T_f	temperature of fluid/ heat carrier [°C]
T_i	inlet temperature relative to ambient temperature [K]
T_o	outlet temperature relative to ambient temperature [K]
T_p	temperature of plate facing the sun [°C]
T_s	stagnation temperature [°C]
$\bar{T}$	mean value of heat carrier temperature [°C]
T'	temperature at the border between glazed and unglazed region relative to ambient [K]
U_b	back loss coefficient [$W/(m^2K)$]
U_L	collector overall loss coefficient [$W/(m^2K)$]
U_t	top loss coefficient [$W/(m^2K)$]
v	magnitude of heat carrier velocity in the upstream region [m/s]
$\dot{V}$	volume flow rate [m^3/s]

Greek letters

α	absorptance of absorber material
η	efficiency
η_0	efficiency for $\bar{T} = T_a$
ρ	density [kg/m^3]
σ_m	standard deviation of the mean
τ	transmittance of glazing
χ	reaction rate

Chapter 1

Introduction

There are strong indications that the effect of human activity since 1750 has led to a net global warming, and that the use of fossile energy ressources must be reduced in order to prevent irreversible climate changes (IPCC, 2007). The consequences of global warming are worsening with increasing temperature change. Some of the regional impacts associated with global warming are increased water stress, sea level rise and loss of biodiversity and food security. The world has an increasing energy demand due to economical and population growth, and today's energy supply is based primarily on fossil fuels, which are responsible for the majority of greenhouse gas emission. The global warming can be reduced by reducing the emission of greenhouse gases and hence there is a need for developing and improvement of methods for utilizing renewable resources (IPCC, 2007).

Energy from the sun can be converted to electricity with the use of solar cells or by concentrating solar power. In addition the radiant energy from the sun can be converted to heat by the use of solar collectors. In a solar collector an absorber converts radiation from the sun to heat, and the heat is transferred to a circulating heat carrier as it passes through the absorber. Heat contains less exergy than electricity, and can hence be regarded as energy with lower quality than electricity. Approximately 40 percent of the end-user energy consumption in EU25 is moderate temperature heat (Rekstad, 2007). This demand does not require high quality energy. Taking this into account there is a large potential for reducing the use of fossile fuels for instance by reducing the use of electric water heaters and oil burners by utilizing the energy from the sun. The International Energy Agency [IEA] has calculated that the amount of energy savings that glazed and unglazed solar collectors contributed with by the end of 2010 approximately corresponds to 53 million tons of CO_2 per year (Weiss & Mauthner, 2012). This is comparable to Norway's annual emission of greenhouse gases (Statistisk Sentralbyrå, 2013). 55 countries, with an installed capacity corresponding to more than 90 percent of the

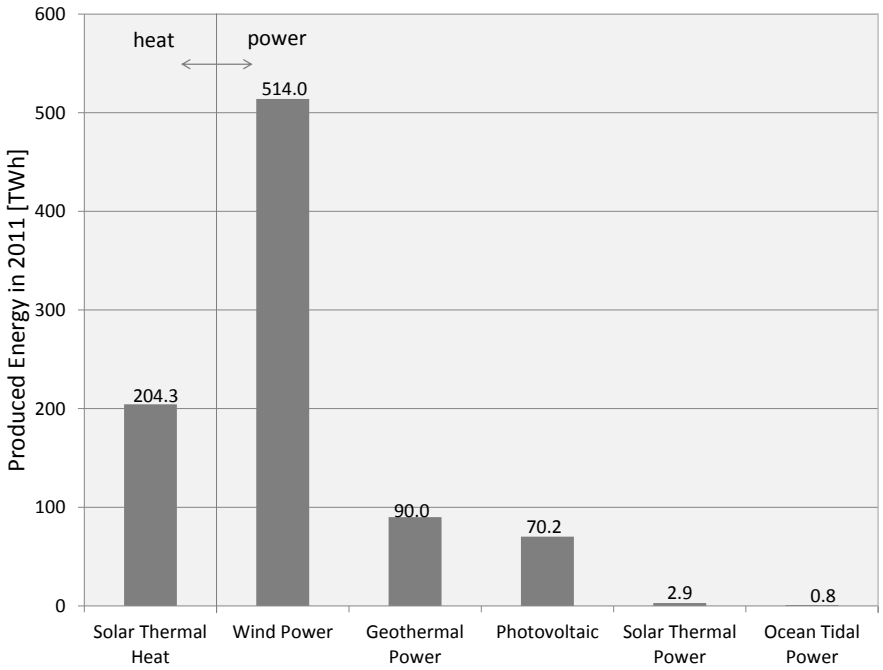

Figure 1.1: *Annual energy generated. Modified figure by Weiss and Mauthner (2012).*

global solar thermal marked was taken into account in these calculations.

To get a grasp of how widespread solar thermal heat is today, some figures are presented here. The total solar thermal energy produced in 2011 was 204.3 TWh (Weiss & Mauthner, 2012). Figure 1.1 shows the production from different renewable sources, with solar thermal heat being second largest next to wind power. Together the energy sources presented in the figure accounted for 4.9 percent of the final energy consumption in 2010 (REN21, 2012). The installed capacity of the respective sources are growing rapidly and in 2011 the capacity of solar heating (excluding unglazed swimming pool heating) increased by 27 percent. Evacuated tube collectors and flat plate collectors are the two dominating solar collectors on the marked with an installed capacity of 56.6% and 31.7% respectively. China is the world leader in total installed capacity in operation and has a marked focusing very much on evacuated tube collectors (Weiss & Mauthner, 2012). Actually China alone acconts for approximately 98% of the evacuated tube capacity. Flat plate collectors dominate in seven of the ten leading countries in terms of installed capacity (Weiss & Mauthner, 2012). Thus the distribution of flat plate collectors is broader than the distribution of evacuated tube collectors.

Solar collectors with high efficiency are on the marked today, but economically these have difficulties competing with conventional energy. According to Tsilingiris (2002, p. 137) the future of this technology depends on the development of "simple, reliable and low cost systems, employing widely available recyclable materials". The potential for cost reduction has motivated the development of solar collector components made of polymer materials.

The temperature in solar collectors may exceed the boiling temperature of the heat carrier. As boiling can damage the collector it must be avoided and this is normally done by letting the heat carrier drain from the absorber and back into the tank. Rekstad (2013) has proposed a new design which is thought to prevent the heat carrier from boiling. The new design is a natural circulating system with a passive heat control, referred to as the Duo-Collector.

Initially the plan was to investigate and estimate the service life of an absorber material on component level. Due to the absence of quantitative results the aim of the work was expanded to include studies of performance related aspects of a partially glazed, natural circulating flat plate collector. The present work therefore consists of two parts. The aim of the first part is to investigate an absorber produced from a new material in order to determine if it is feasible for solar thermal applications. The material should sustain the thermal conditions in a solar collector, have an absorptance which maintains good efficiencies and show good dimensional stability in order to be feasible. The absorber is designed by Aventa and extruded by Kaysersberg Plastics from a polypropylene material produced by Borealis and is presented as a candidate for use in flat plate collectors.

Since the processing of the absorber sheets may affect the material, the tests are performed on component level. Standard tests are not applicable on the given design, and therefore a test procedure developed at the University of Oslo and later taken in use by others is used. The samples to be tested are extruded into absorber sheets and are tested for mechanical, dimensional and optical changes. The changes in the material's properties during heat exposure are investigated for two different temperatures. Mechanical changes are mapped using an indentation test investigated by Olivares (2008). The test procedure characterize the stability and strength of the internal structure as well as the surface of the tested specimens (Olivares, 2008).

The aim of the second part is to develop a simulation program and use it to predict the maximum temperatures obtainable in a Duo-Collector and investigate the performance of such a system. The efficiency, flow velocity and temperature

increase of the heat carrier is calculated for different operating conditions.

Chapter 2

Solar heating systems

2.1 Studies on low cost systems

Effort is made to reduce the cost of solar water heating technology. According to Alghoul, Sulaiman, and Azmi (2005) polymers are pointed out as a promising alternative because they are cheap relative to metal, widely available, are lightweight and are tolerant to corrosion and freezing temperatures. A disadvantage of using polymers is their low thermal conductivity varying slightly around 0.2 W/(mK) (Tsilingiris, 1999). The design of the collector should seek to overcome this obstacle. According to Tsilingiris (2002) the most promising design is the extruded parallel polymer plate absorber design, as it allows extended wetted surfaces of the absorber. In order to optimize the collector efficiency the thickness of the top plate should be minimized, but the plate has to be able to withstand hydrostatic loads and provide sufficient mechanical rigidity. With plate thickness smaller than typically about 1 to 1.5 mm the collector efficiency factor will be higher than approximately 0.96 (Tsilingiris, 1999). In a later paper Tsilingiris (2002) investigated a back absorbing parallel plate polymer absorber, where the top plate is transparent, and the solar radiation is absorbed by the water stream and by the back plate. He developed a theoretical analysis for evaluation of the design. Compared to a top absorbing design the author found that the instantaneous collector heat collection efficiency increase in the order of 14%.

Flat plate collectors have been studied by many researchers and the theory is extensively presented by Duffie and Beckman (2006). This theory is based on the assumption that temperature gradient through the absorber metal sheet is negligible. This does not apply to polymeric absorbers, and for the extruded parallel polymer plate absorber design Tsilingiris (1999) performed an analysis and adjusted the performance parameters.

Another design is studied by Chaurasia (2000). This collector consists of a network of aluminum pipes embedded in concrete slabs, and are intended to cover building roofs. These unglazed collectors are low-cost and have operating temperatures varying between 36 °C and 58 °C. An analysis and performance of another low-cost solar heater has been investigated by Siqueira, Vieira, and Damasceno (2011). The solar collector studied is a Low-Cost Solar Heater (LCSH) made entirely of polymeric materials. It is composed of uncovered flat panels of rigid PVC. The article authors compare the efficiency of the collector with that of a conventional solar heater composed of a glass-covered copper collector and a stainless steel tank. The results indicated that the LCSH presented a good thermal performance in terms of heat loss as well as efficiency and temperature values attained. Although the LCSH is not as efficient as the conventional heater the authors recommends it as a good alternative for heating water. It is also concluded that there is a potential for significant economical savings when electric showers are replaced with a LCSH.

There has still not been done much research on the reliability, durability, and long-term performance of polymeric materials for solar collector applications (Alghoul et al., 2005). The research group at the University of Oslo has tested a variety of polymer materials. The group has also developed and investigated a test procedure for quantifying the mechanical degradation in absorber sheets caused by heat exposure (Olivares, 2008; da Silva, 2008). This test procedure has also been taken into use by the Polymer Competence Center Leoben, Austria, the Institute of Polymeric Materials and Testing at the Johannes Keppler University, Linz Austria, Saudi Basic Industries Corporation (SABIC; former General Electric Plastics) and Fraunhofer Institute for Solar Energy Systems ISE, Germany (Meir, 2013).

An extruded triple-wall sheet made of a polyphenylene/polystyrene blend (PPE/PS) has been investigated by Olivares, Rekstad, Meir, Kahlen, and Wallner (2008, 2010). In another study mechanical tensile tests were performed on thin films made of different materials with a thickness of approximately 500 μm. The materials tested were a polyphenylene ether polystyrene blend (PPE + PS), polycarbonate (PC), two semi-crystalline polymers named polyamid 12 (PA12), two types of crosslinked polyethylene (PE-X) and two types of polypropylene (PP) (Kahlen, Wallner, & Lang, 2010a, 2010b). Absorbers made of polyphenylene sulfide (PPS) have also been investigated (da Silva, 2008). Some of the results from these studies are presented in Appendix A and will be compared to the results obtained in the present study. The polypropylene blend investigated in the present work has not been tested previously.

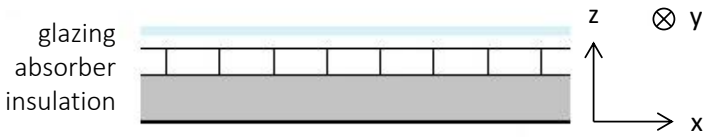

Figure 2.1: *Schematic cross section of a flat plate collector.*

2.2 Flat plate collectors

Description

The schematic diagram presented in Figure 2.1 illustrates the main parts of a glazed flat plate collector. The absorber sheet in the figure has an extruded parallel polymer plate absorber design, which consists of two parallel polymer plates connected with inner walls. The inner walls divide the space between the parallel plates into multiple channels. Solar radiation passes the glazing and is converted to heat by the absorber. The heat carrier flows through the absorber channels, allowing heat to be transferred from the absorber to the fluid. The transparent cover, or glazing, acts as a heat trap for infrared radiation (Alghoul et al., 2005). The glazing reduces convection and radiation losses from the absorber to the surroundings, and the thermal insulation reduces conduction losses (Duffie & Beckman, 2006). It also protects the absorber from adverse weather conditions. (Alghoul et al., 2005).

Unit area heat rate

The heat rate at which energy is transferred from the sun to the heat carrier both depends on and changes the heat carrier temperature. In a region with uniform heat carrier temperature and during steady state conditions the unit area heat rate q_u, measured in $\mathrm{W/m^2}$, is given by

$$q_u = F'[S - U_L(T_f - T_a)], \tag{2.1}$$

with

$$F' = \frac{1}{1 + U_t/H},$$

and

$$U_L = U_t \left(1 + \frac{1}{1 + (H/U_b)}\right) + U_b \left(1 + \frac{1}{1 - (H/U_b)}\right),$$

for

$$H = \frac{k_p}{b}.$$

In these equations U_L is the overall heat loss coefficient, T_f is the heat carrier temperature, T_a is the ambient temperature, U_b and U_T are heat loss coefficients for the base an top and b and k_p are the thickness and the thermal conductivity of the plate respectively (Tsilingiris, 1999). S is the solar radiation absorbed by the collector per unit area absorber. For a glazed absorber S can be approximated as

$$S \approx G\alpha\tau 1.01,$$

where G is the solar irradiance incident on the collector surface, α is the absorptance of the absorber sheet and τ is the transmittance of the glazing. The solar irradiance is measured in $\mathrm{W/m^2}$ and describes the rate of radiant solar energy incident on a surface per unit area (Duffie & Beckman, 2006). For an unglazed collector S is given as

$$S = G\alpha$$

The expression in the square brackets in Eq. (2.1) represents the difference between the absorbed solar radiation and the thermal energy loss due to conduction, convection and infrared radiation (Duffie & Beckman, 2006). During operation the temperature of the heat carrier in the absorber will vary with location, implying that the unit area heat rate q_u will vary with location.

Collector Efficiency

The efficiency η is a measure of the performance of the collector. It is defined as the ratio between the total useful gain delivered to the heat carrier during a specified period of time and the solar energy incident on the collector during the same period of time and is given by

$$\eta = \frac{\text{Total useful gain}}{\text{Solar energy received}} = \frac{\int Q_u \, \mathrm{d}t}{A \int G \, \mathrm{d}t}. \tag{2.2}$$

In the literature the useful energy gain usually shows a first or second order dependency on the temperature difference between the mean heat carrier temperature

and the ambient temperature (Morrison, 2001; Duffie & Beckman, 2006). Assuming stationary conditions a second order expression for the efficiency is approximated by (Morrison, 2001):

$$\eta = \eta_0 - \frac{k_1(\bar{T} - T_a)}{G} - \frac{k_2(\bar{T} - T_a)^2}{G}, \tag{2.3}$$

where η_0, k_1 and k_2 are constants which can be fitted experimentally and $\bar{T}$ is the mean heat carrier temperature.

2.3 Thermosyphon systems

Description

Solar collectors can be active or passive. The passive systems are also referred to as thermosyphon systems (Duffie & Beckman, 2006). In contrast to active solar systems, thermosyphon systems do not use mechanical devices, such as for instance electrical pumps or fans, to collect and transfer heat. Approximately three quarters of installed solar collector systems are thermosyphon systems (Weiss & Mauthner, 2012). The design shown in Figure 2.3 is a thermosyphon system. These systems use natural convection as the driving force for the circulation of water. The density of water decreases as the temperature rises, which causes the water in the collector to rise into the tank as it is heated. As the circulation is governed by temperature gradients in the tank, the circulation flow rate is naturally in phase with the radiation level (Morrison, 2001). Under hard-water conditions a common problem is scaling. Scaling occurs on polymer materials in about the same rate as on copper and in a thermosyphon system it will reduce the flow rate due to increased hydraulic resistance (Duffie & Beckman, 2006).

Volume flow rate

The volume flow rate $\dot{V}$ is a measure of the rate at which the heat carrier flows through the collector array. It is defined as the volume of heat carrier which passes through the system per unit time. In an active system this can be regulated by adjusting the pump. The amount of temperature increase through the collector varies with the flow rate. A low flow rate results in a larger temperature increase through the collector because the time it takes the heat carrier to pass through the collector is increased. If the flow rate is sufficiently low, stratification of the temperature in the tank will occur. Cold water from the bottom of the tank will feed the collector and the heated water will enter the top of the tank and stay

there. Stratification is important because this reduces the inlet temperature to the collector leading to a higher collector efficiency (Rekstad & Meir, 2012). Also, the temperature in the top of the tank will be higher when the temperature distribution is stratified, leading to hotter tap water. In a system with a high volume flow rate the water in the tank will have a homogeneous temperature distribution. The maximum temperature will hence be lower, but on the other hand the heated volume will be larger, allowing delivery of heated water for a longer time period.

The temperature rise through natural-convection systems has been observed to be constant under a wide range of conditions. For well designed systems without serious flow restrictions the increase is observed to be approximately 10 °C (Duffie & Beckman, 2006). In a thermosyphon system the circulation is due to density differences of the heat carrier in the system. The flow rate is governed by the useful gain of the collector which produces temperature differences leading to the density differences (Duffie & Beckman, 2006). Modelling a specific system requires iterative calculations because the temperatures and flow rates are interdependent (Duffie & Beckman, 2006).

The volume flow rate $\dot{V}$ is given by

$$\dot{V} = \frac{dV}{dt} = Av,$$

The pressure P_1 at the bottom of a water column with height h is given by

$$P_1 = P_0 + \frac{mg}{A_c},$$

where P_0 is the pressure at the top of the column, m is the mass of the water column, g is the gravitational constant and A is the cross section area of the column. In a column of constant temperature the density is constant and pressure is given by

$$P_1 = P_0 + \rho g h. \tag{2.4}$$

2.4 Heat carrier temperature

A flat plate collector exposed to a constant amount of solar irradiance and a constant ambient temperature for a sufficient amount of time will reach equilibrium. During equilibrium the amount of energy absorbed by the system is equal to the

sum of the energy lost to the ambient and the useful energy delivered by the system.

Solving Eq. (2.3) with respect to $\bar{T} - T_a$ gives

$$\bar{T} - T_a = \frac{1}{2}\left(-\frac{k_1}{k_2} + \sqrt{\left(\frac{k_1}{k_2}\right)^2 - \frac{4G \cdot (\eta - \eta_0)}{k_2}}\right). \tag{2.5}$$

For a given collector, η_0, k_1 and k_2 are constants. Assumptions about the efficiency gives us the mean temperature of the heat carrier relative to the ambient solely from the irradiance.

During stagnation the amount of energy absorbed by the system is equal to the energy transferred to the ambient. The stagnation temperature T_s is the temperature of the heat carrier during stagnation when the system does not deliver any energy. Thus no net energy is transferred through the top plate of the collector and the temperature of the heat carrier stays unchanged as it passes through the collector. By inserting $\eta = 0$ and $\bar{T} = T_s$ in Eq. (2.5) we find

$$T_s - T_a = \frac{1}{2}\left(-\frac{k_1}{k_2} + \sqrt{\left(\frac{k_1}{k_2}\right)^2 + \frac{4G\eta_0}{k_2}}\right).$$

Figure 2.2 shows typical stagnation temperatures for a glazed and an unglazed collector (Weiss & Mauthner, 2012; Rekstad, 2013).

2.5 The Duo-Collector

The Duo-Collector is a partially covered flat plate collector. The heat carrier in a glazed solar collector can exceed the boiling temperature. Boiling may damage the collector, and must therefore be avoided (Duffie & Beckman, 2006). Active systems can be designed to let the heat carrier in the absorber drain back into the tank in order to prevent damage from boiling or freezing.

The new approach to this problem is to design the collector in such a way that the maximum temperature achievable will be below the boiling point of the heat carrier. The stagnation temperature for an unglazed collector is below the boiling point of water for all ambient conditions, while a glazed collector exceeds it for a large range of conditions. By only covering a fraction of the absorber with glazing it is expected that the maximum temperature achievable will lie between the stagnation temperature of a glazed and an unglazed collector.

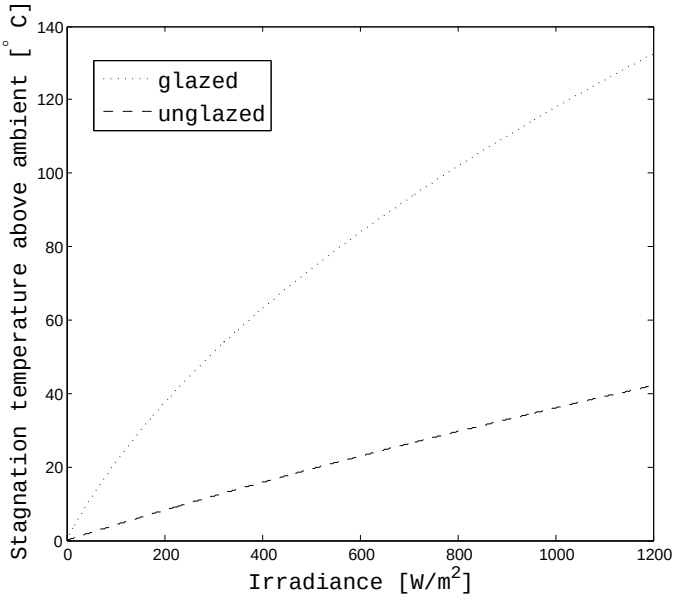

Figure 2.2: *Temperature above ambient of the absorber during stagnation. The temperature of the absorber is found by adding the ambient temperature.*

The investigated design is shown in Figure 2.3. The absorber consists of 55 parallel channels. The detailed view to the right shows that the five outermost channels on both sides are used to transport the heat carrier from the tank to the bottom of the absorber. These channels are shorter to allow cold water from the base of the tank to feed the collector. The upstream channels in the center are longer, letting the heated water enter the top of the tank.

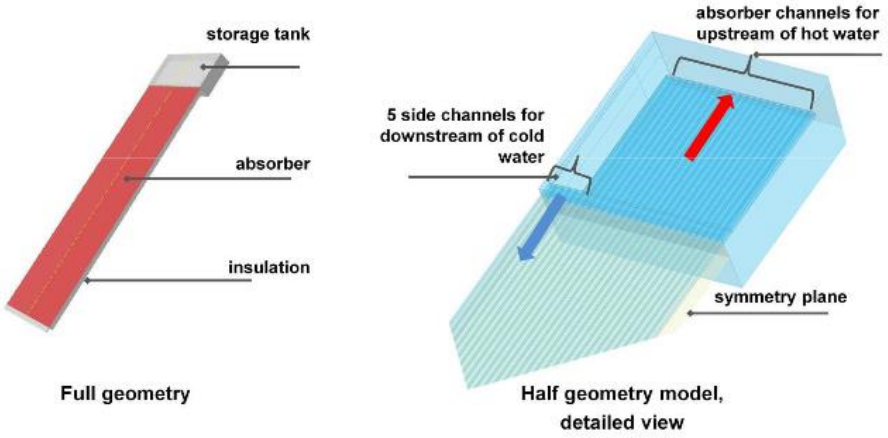

Figure 2.3: *Design of the thermosyphon collector used in the simulation (HTCO GmbH, 2012).*

Chapter 3

Polymer science

3.1 Polypropylene

Polypropylene (PP) is a thermoplastic material with a semi-crystalline structure. Thermosplastics are a sub group of plastics and they are characterized by the fact that they soften when heated and harden when cooled. This allows them to be processed easily into various shapes (Wallner, Lang, & Schnetzinger, 2012; Resch & Wallner, 2012). The absorber sheets are produced by an extrusion process, where the raw material is melted, shaped in a die and then rapidly cooled down by a calibrator. This process exposes the material to high pressure and rapid temperature changes.

Figure 3.1 shows a classification of thermoplastics by structure, temperature performance and price (Plastics Europe Market Research Group, 2011). PP can be found in the bottom right cell of the pyramid. The figure shows that PP is a low cost polymer material and is expected to tolerate temperatures up to 100 °C. It is also of interest to point out that the material currently used in glazed flat plate collectors produced by Aventa is a modified PPS material, which can be found in the top right cell.

3.2 Elasticity and plasticity

Elasticity and plasticity describes the deformation of a material when it is subject to stress. Figure 3.2 shows a typical stress-strain diagram for tensile stress. The first part of the curve has a linear behavior indicating that the deformation obeys Hooke's law. Point b in the figure indicates the elastic limit. Deformation until this point is reversible and beyond this point the deformation is permanent.

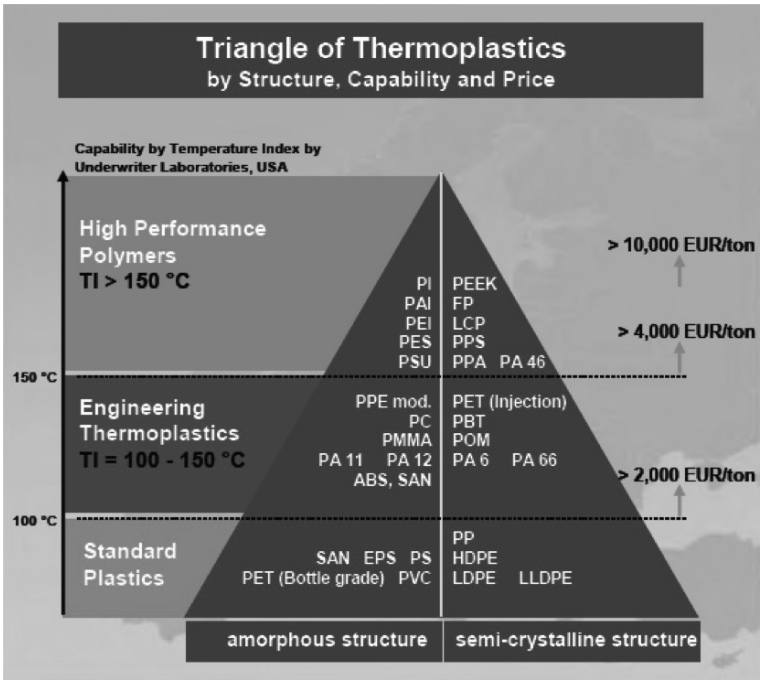

Figure 3.1: *Classification of thermoplastics by structure, capability and price (Plastics Europe Market Research Group, 2011).*

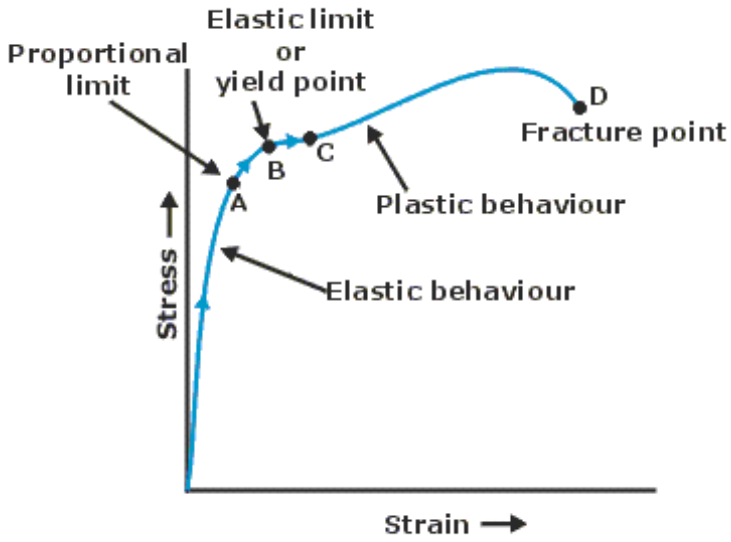

Figure 3.2: *Typical stress-strain diagram for tensile stress.*

Further stress will eventually lead to fracture of the material (Young & Freedman, 2004). Ductile materials will undergo a large amount of plastic deformation before the fracture point is reached. Brittle materials will fracture after a small amount of plastic deformation. The slope of the linear region is called Young's modulus which is a measure of the stiffness of the material. A steep behavior indicates that a small deformation requires a large amount of stress. Large values of Young's modulus indicate high stiffness. If compression is caused by an applied load the deformation is characterized by the penetration depth of the load. The magnitude of Young's modulus is defined in the same way for both tensile and compressive stress (Young & Freedman, 2004). A diagram showing compressive load vs. compressive extension will have the same characteristics as a compression stress vs. strain diagram because the load is proportional to the stress and the extension is proportional to the strain.

3.3 Ageing

Polymer ageing is a term used for the changes in a material's properties over a period of time (White, 2006). The thermal ageing that takes place in thermoplastic polymers when the environmental temperature is below the melting temperature is explained by referring to changes in the morphology of the polymer structure

(Kim, Lee, & Tsai, 2002). White (2006) presents a categorization of the different ageing processes occurring in polymers. He points out that the subject of ageing in polymers is vast, and that the categorization he makes is not sufficient to categorize all topics. Still the basic features are of interest and will be presented here.

The extrusion process gives rise to physical ageing of thermoplastic polymers. The rapid cooling after the extrusion process does not leave the final product in thermodynamic equilibrium. During the rapid cooling the material reaches thermal equilibrium with the environment. The material needs longer time to reach thermodynamic equilibrium and the low conductivity of polymers causes the formation of a strong temperature gradient. As a result the volume of the material is larger than it otherwise would be. The physical ageing occurs during an extended ageing period. Molecular relaxations over time slowly draws the material closer to equilibrium, resulting in a gradual increase of the material's density. By increasing the ageing temperature of a polymer the physical ageing may be accelerated (White, 2006).

The various changes occurring in the material due to elevated temperatures, including the acceleration of physical ageing, are collectively known as thermal degradation. Oxygen is an aggressive chemical, which can result in scissioning and crosslinking of the chains constituting the polymer. The rate of these reactions are temperature dependent and may be negligible at ambient temperatures. However, at elevated temperatures these reactions may occur, leading to embrittlement of the material (White, 2006).

3.4 Mathematical model of degradation

The approach which is used to describe the degradation of the absorber material at different temperatures is the Arrhenius approach. By modelling the chemical processes occurring as one overall chemical process, the relation between the reaction rate χ and the temperature T in Kelvin can be expressed by:

$$\chi(T) = Ce^{-\frac{E_a}{kT}}, \tag{3.1}$$

where C is a proportionality constant, E_a is the activation energy for the reaction and k is the Boltzmann constant. This gives a degressive rate, which means that the slope of the the rate is decreasing with increasing temperature. According to Bockhorn, Hornung, Hornung, and Schawaller (1999) this is often the case with the ageing process of plastics. To determine the reaction rate data from two different temperatures are necessary. In practice it is usual to collect data for more

than two temperatures, and use a least-squares fitting procedure to determine the constants (Metiu, 2006).

A semi-empirical model can be used to find fitted, non-experimental values for different temperatures. The model proposes that apparent mechanical changes in the polymer reflects the changes in the molecular structure (Olivares, 2008). It is assumed that molecular changes result in mechanical changes and compressive tests are used as the degradation parameter. The load F needed to bring the material to its fracture point depends on exposure temperature T and duration of the exposure t. The following relation is assumed

$$\frac{dF}{dt} = -\chi(T)F^n. \tag{3.2}$$

Here the parameter n is the reaction order. According to (Rekstad & Meir, 2010) good fits are normally obtained with values of n between 1 and 2. For simplicity $n = 1$ and $n = 2$ will be used. Solving Eq. (3.2) for $n = 1$ gives

$$F(T,t) = \frac{F_0}{e^D}$$

and $n = 2$ gives

$$F(T,t) = \frac{1}{D + 1/F_0},$$

where F_0 is the load needed to bring unexposed material to its fracture point, and D is the thermal dose given by

$$D = \int \chi(T)dt.$$

Assuming constant temperature gives

$$D = \chi(T)\Delta t.$$

Figure 3.3 qualitatively shows how the load at failure changes with exposure time for two different temperatures $T_1 > T_2$. In the figure the solid straight lines indicate that when the temperature is increased the exposure time needed for a given critical load is decreased. The dotted line shows that for a constant temperature the exposure time is reduced when the critical load is increased.

3.5 Service life estimations

During operation the absorber is exposed to hydraulic pressure and differences in dilation due to temperature gradients or due to cyclic stress during day and night.

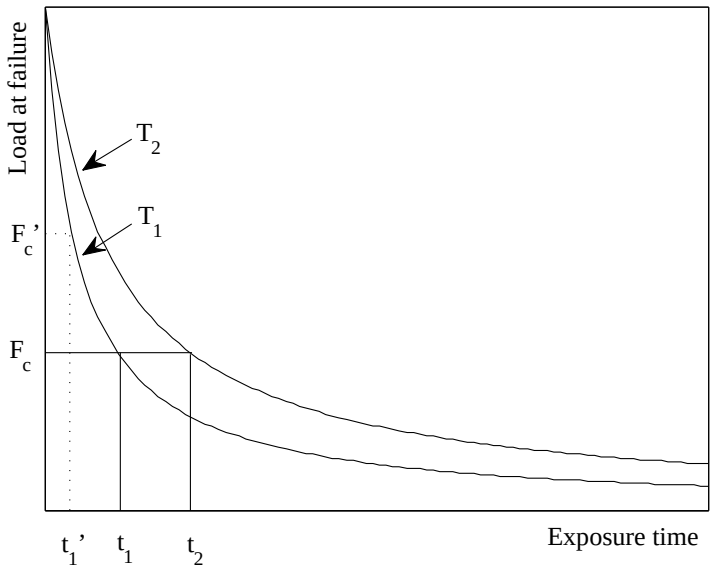

Figure 3.3: *Qualitative representation of how load at failure changes with exposure time and temperature.* $T_1 > T_2$

Before operation load is applied as a result of handling of the absorber during manufacturing and installation. In order to estimate the service life of the absorber a criteria for failure must be introduced. The criteria for failure can be defined as the critical load F_c which the absorber should be able to withstand (Olivares, 2008).

For the temperature T_1 Figure 3.3 shows that there is a time t_1 corresponding to the critical load F_c. Likewise there is a time t_2 for the temperature T_2. According to the theory the thermal dose D is the same for specimens with the same critical load. Therefore the critical thermal dose D_c associated with the critical load F_c can be expressed as

$$D_c = \chi(T_1) \cdot t_1 = \chi(T_2) \cdot t_2.$$

By implementing Eq. 3.1 this brings us to the following result

$$E_a = \frac{k \cdot \ln\left(\frac{t_1}{t_2}\right)}{\frac{1}{T_1} - \frac{1}{T_2}}$$

Once E_a is determined the theory allows us to predict the degradation occurring at the temperature T_i. The time t_i needed to give the material the critical thermal dose D_c is given by

$$t_i = t_1 e^{\frac{E_a}{k}\left(\frac{1}{T_i}\frac{1}{T_1}\right)}$$

Chapter 4

Experimental setup

4.1 The alphameter

The alphameter is a device used to measure the solar absorptance of a surface. It is constructed for measurements of opaque solar absorbers, and delivers rather precise measurements for this purpose. The device consists of an integrating sphere, five light sources and two detectors. The integrating sphere act as a diffuser. Opposite the detectors there is a hole in the sphere surface, in which the specimen to be tested is placed. The integrating sphere is illuminated subsequently by the light sources: blue, green, red and infrared light-emitting diodes (LEDs) and a tungsten halogene lamp. The reflected LED signals are measured by a collimated silicon detector, while the reflected tungsten halogene signal is measured by a collimated germanium detector (Optosol, 2002). For opaque surfaces the absorption can be found from the reflectance since the energy is either absorbed or reflected (Duffie & Beckman, 2006). The absorptance is hence measured as the complimentary part of the reflectance.

The alphameter operates in a wavelength region of $0.3 - 1.4$ μm, which contains most of the solar radiation received at the surface of the earth. It has a reproducibility $< 0.5\%$ (Optosol, n.d.) which means that the difference between two measurements will be less than 0.5% with a probability of approximately 0.95.

4.2 The Instron 3345 machine

The Instron 3345 machine is an instrument used for mechanical testing. For compression tests, the samples are placed on a compression plateau, and are compressed by a brass indenter. Figure 4.1 shows a schematic representation of the brass indenter with dimensions and Figure 4.2 shows a picture of a sample being

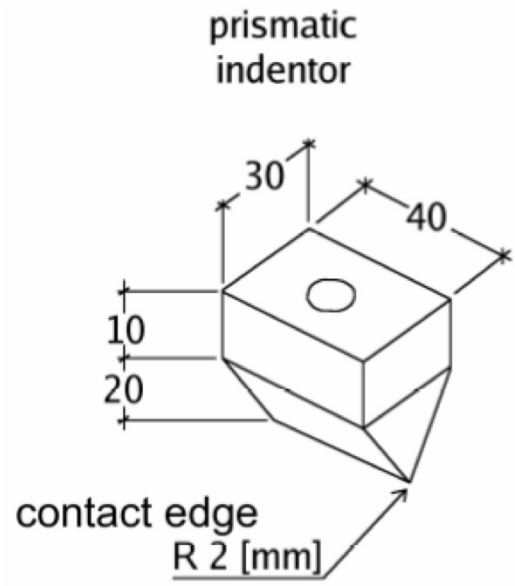

Figure 4.1: *The brass indenter of the instron 3345 machine.*

tested. The indenter is connected to a load cell, converting the force it is exposed to into an electrical signal. The speed at which the indenter is moving and the position at which it will stop is programmed by the user. The testing produces a stress-strain diagram which can be interpreted by the information given in Section 3.2.

4.3 Termaks heating cabinets

Two Termaks heating cabinets are used for the heat ageing in form of a dry heat load. The ovens are of model TS 8056 and TS 8024. The difference between these models is the size of the ovens. TS 8056 is the larger, and will be referred to as the large oven, while TS 8024 will be referred to as the small oven. The spatial and time deviation of the temperature in the ovens while empty is ± 1.5 °C and ± 1 °C respectively (Termaks, 2013).

4.4 Absorber material and design

The specifications of the absorber material presented here are taken from the producer's data sheet. The material is a polypropylene heteroplastic copolymer named BA160E-8229-01. It is produced by Borealis and designed for injection molding

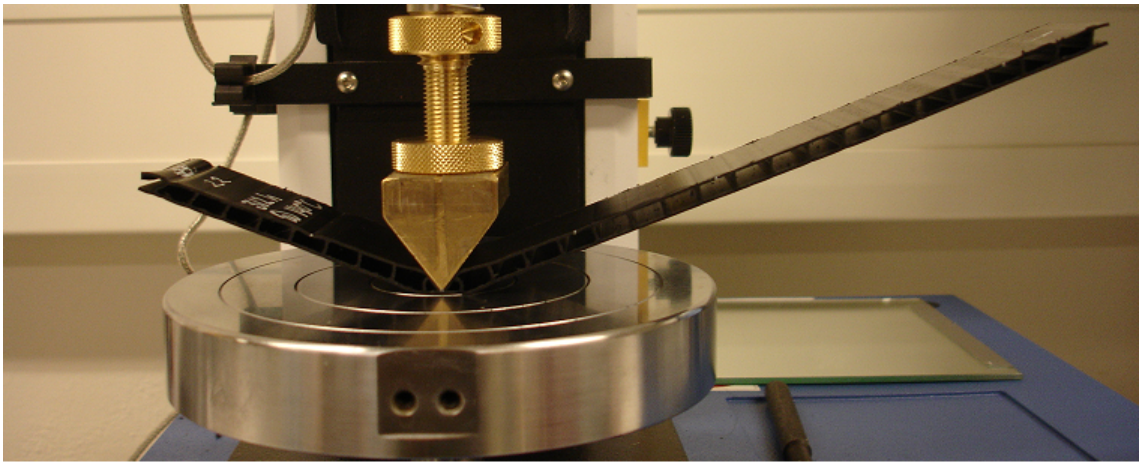

Figure 4.2: *Indentation test of a sample with the instron 3345 machine.*

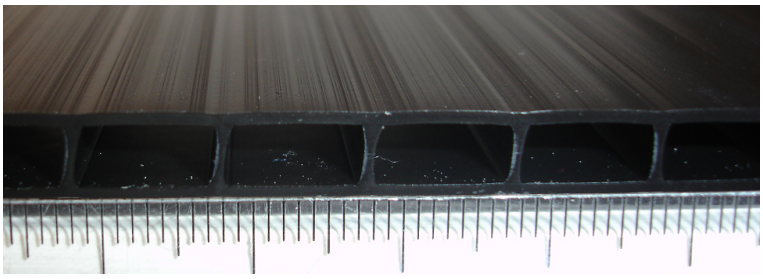

Figure 4.3: *The profile of the extruded sheet photographed with a plastic ruler.*

and extrusion (Borealis, 2013). It can be used for applications involving drinking water and irrigation. The absorber sheet is produced by an extrusion process as described in Section 3.1. The profile of the sheet next to a plastic ruler is shown in Figure 4.3. The dimensions of the aperture between the plates and the inner walls are approximately (10×4) mm. The material is expected to have a shrinkage of $1-2\%$, depending on wall thickness and moulding parameters. The density of the material is 900 kg/m^3 and the melting temperature is $230-260$ °C.

On one side of the sheet used in this work the surface is smooth, whilst the other surface does not have a satisfactory finish. These sides will respectively be referred to as the top and the bottom of the sheet. Figure 4.4 shows a picture of the top and bottom of the sheet next to each other.

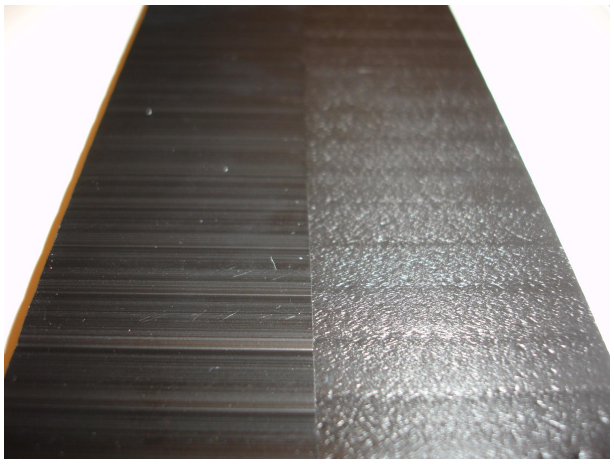

Figure 4.4: *The top (left) and bottom (right) surface of the extruded sheet.*

Chapter 5

Experimental studies

5.1 Approach

The samples

All experimental tests were performed with samples cut from the same extruded sheet having a thickness of approximately 6 mm. The edges of the sheet were trimmed, and then the sheet was cut into three sections corresponding to an absorber with of 54 cm. One of these sections was divided into two subsections, which were used to produce samples with a dimension of approximately 40 mm $\times$270 mm. Figure 5.1 shows the samples' original position in the extruded sheet and Figure 5.2 shows a photo of one sample. The direction of the intrinsic absorber channels can be seen by the pattern on the surface in Figure 5.2. In Figure 5.1 the channels are directed vertically. The samples were labeled with a number and a letter. Samples whose short ends were originally connected were given the same number and together these are referred to as a sample pair. One sample pair is colored dark gray in Figure 5.1. Samples from the outermost subsection were labeled A, samples from the other subsection were labeled B. For details on the material see Section 4.4. Each sample contains 27 intact channels. These were numbered $1-27$ for samples labeled A and $28-54$ for samples labeled B, counted from left to right in Figure 5.1.

Heat ageing

Fifteen sample pairs were exposed to heat ageing in the large heating cabinet, which was heated to 140 °C. The exposure times of these samples can be seen in Table 5.1. Another 15 sample pairs were exposed to heat ageing in the small heating cabinet, which was heated to 150 °C. The exposure times for these samples

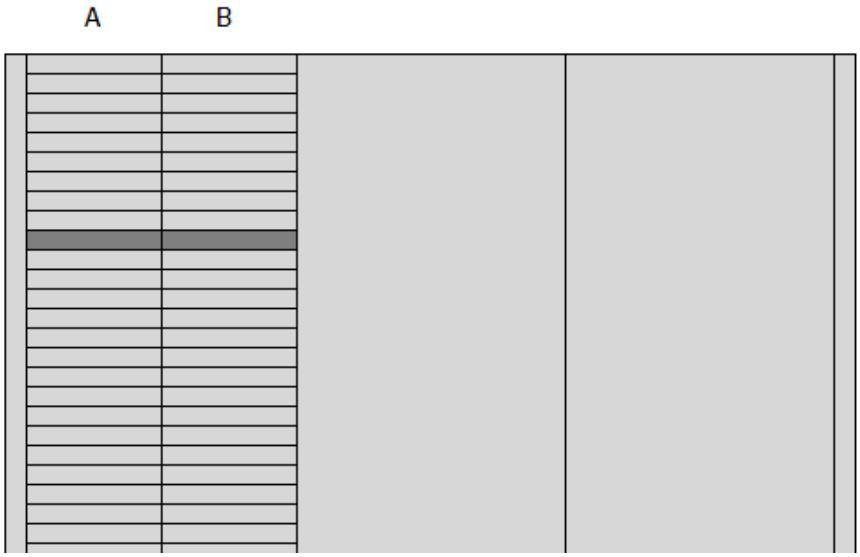

Figure 5.1: *Schematic figure showing the sample's original position in the extruded sheet*

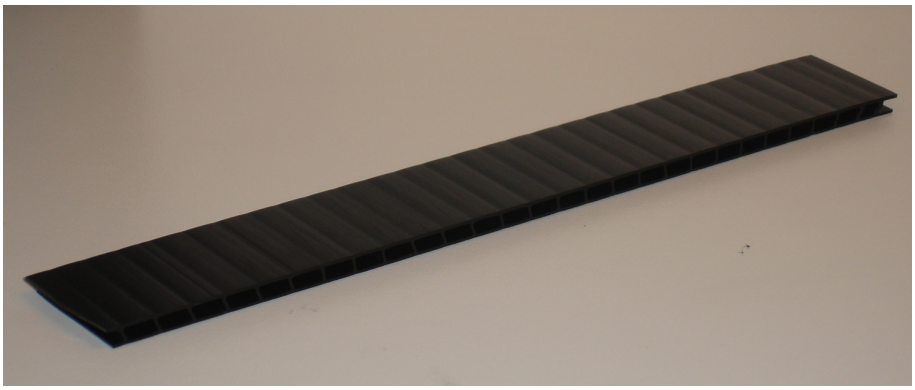

Figure 5.2: *Picture of one of the absorber samples.*

Table 5.1: *Exposure times and corresponding sample numbers for absorber samples exposed to heat ageing at* 140 $^{\circ}C$*. Indentation tests were carried out on the samples marked with a checkmark.*

Exposure time	Sample label	Exposure time	Sample label
4 days = 96 h	1B✓	34 days = 816 h	3A
6 days = 144 h	2B✓	37 days = 888 h	4A
8 days = 192 h	3B✓	39 days = 936 h	5A
11 days = 264 h	4B✓	41 days = 984 h	6A
13 days = 312 h	5B✓	44 days = 1056 h	7A
15 days = 360 h	6B✓	46 days = 1104 h	8A
18 days = 432 h	7B✓	48 days = 1152 h	9A
20 days = 480 h	8B✓	51 days = 1224	10A
22 days = 528 h	9B✓	53 days = 1272 h	11A
25 days = 600 h	10B✓	55 days = 1320 h	12A + 12B
27 days = 648 h	11B✓	57 days = 1368 h	13A + 13B
30 days = 720 h	1A	60 days = 1440 h	14A + 14B
32 days = 768 h	2A	62 days = 1488 h	15A✓+ 15B✓

can be seen in Table 5.2. After the exposure the samples were cooled down to room temperature.

Indentation tests

In Table 5.1 and 5.2 some of the sample labels are marked with a tick. This indicates that the given samples were used to perform six indentation tests. In addition to virgin specimens, which were not exposed to heat ageing, were tested. All the indentation tests were performed with the same input parameters. The width of the specimens equal the width of the brass indenter. The speed of the indenter was set to 10 mm/min and the indentation procedure was programmed to end when the penetration depth of the indenter was 5 mm. The tests were performed with the indenter parallel to the channel direction and placed symmetrically between two inner walls. For the indentation tests the smooth surface of the absorber samples was facing downwards. Figure 5.3 shows a sample being tested. White marks were made on both sides of the sample in order to align it with the indenter and one of these can be seen in the picture right below the tip of the indenter.

In Tables 5.1 and 5.2 there are a total of 41 cells, corresponding to 41 different temperature-time conditions. Samples labeled A were tested in channel 5, 9, 13, 17, 21

Table 5.2: *Exposure times and corresponding sample numbers for absorber samples exposed to heat ageing at* 150 °*C. Indentation tests were carried out on the samples marked with a checkmark.*

Exposure time	Sample label	Exposure time	Sample label
4 days = 96 h	16A + 16B✓	22 days = 528 h	24A + 24B
6 days = 144 h	17A + 17B✓	25 days = 600 h	25A + 25B✓
8 days = 192 h	18A + 18B	27 days = 648 h	26A + 26B
11 days = 264 h	19A + 19B	29 days = 696 h	27A + 27B
13 days = 312 h	20A + 20B	32 days = 768 h	28A + 28B
15 days = 360 h	21A + 21B✓	34 days = 816 h	29A + 29B
18 days = 432 h	22A + 22B	36 days = 864 h	30A✓+ 30B✓
20 days = 480 h	23A + 23B		

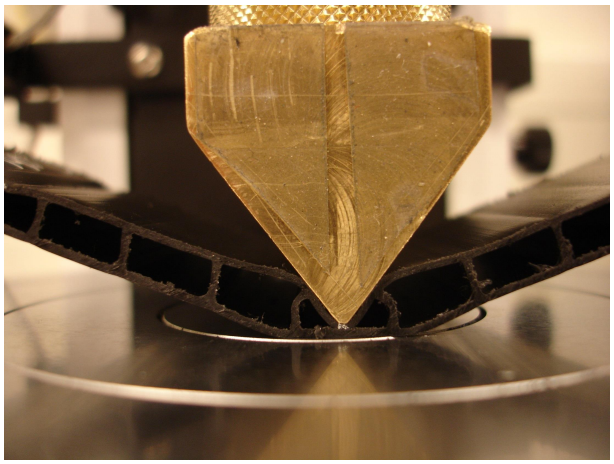

Figure 5.3: *Picture of a sample during an indentation test.*

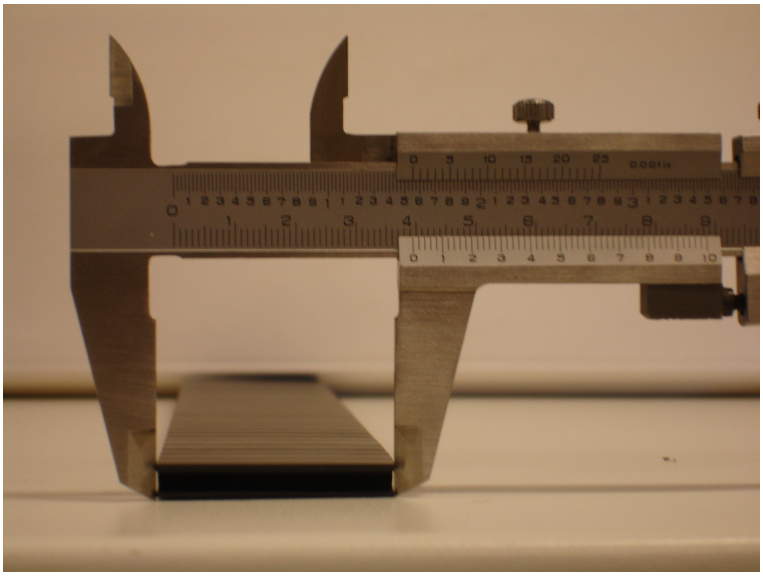

Figure 5.4: *The tips of the caliper's outside jaws touch the supporting surface during measurements.*

and 25. Samples labeled B were tested in channel 30, 34, 38, 42, 46 and 50.

Mapping dimensional changes

The samples labled A and exposed to heat ageing at 150 °C were used to map dimensional changes. Before the samples were exposed to heat the width of the samples was measured at six different locations. Each location was marked with a white pen. The width was measured at the same location after the heat ageing. The measurements were performed with a vernier caliper. The samples were placed on a horizontal flat surface, and the caliper was placed with the tips of the outside jaws touching the surface. This is shown in Figure 5.4. For each sample the mean relative width reduction and the standard deviation was calculated. The relative width reduction was then plotted against the exposure time.

Optical testing

All samples exposed to heat ageing at 150 °C were used to map changes in the absorptance. In addition one virgin sample pair was used. The absorptance was measured with the alphameter described in Section 4.1. A total of 20 absorptance measurements were conducted on each sample pair. The arithmetic mean was cal-

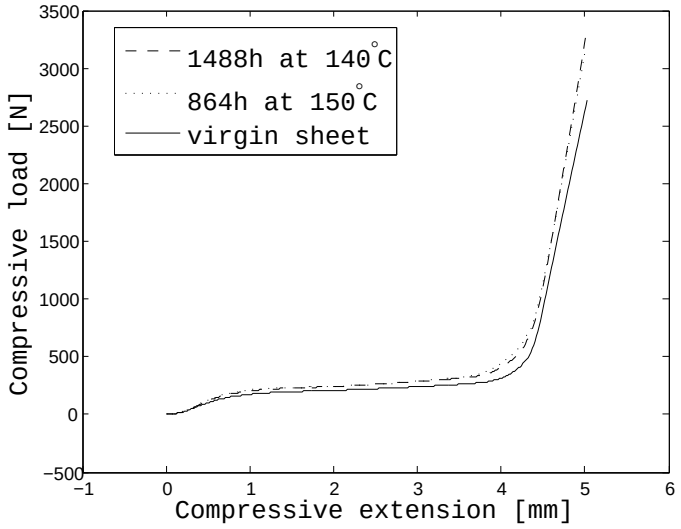

Figure 5.5: *Mean value of stress-strain graphs for indentation test performed on absorber samples from section A.*

culated. The reproducibility of the alphameter is used as a systematic error, while the standard deviation of the mean is used as the random error. The absorptance was plotted as a function of exposure time with the random error.

5.2 Results

Indentation tests

The compressive load vs. compressive extension curves produced by the indentation tests from the unexposed samples and the samples with longest exposure time at 140 °C and 150 °C are presented in Appendix C. The results produced by testing specimens from section A were used to produce the result presented in Figures 5.5 and 5.6. The figures show compressive load vs. compressive extension curves for one sample exposed to heat ageing for 1488 hours at 140 °C, one sample exposed to heat ageing for 864 hours at 150 °C and one virgin sample. Each of the three graphs were produced by calculating the arithmetic mean of the six indentation tests performed. A cut-out of the figure which includes errorbars is shown in Figure 5.6. The error is calculated as $2\sigma_m$ where σ_m is the standard deviation of the mean calculated from the six indentation tests. Failure did not occur for any of the absorber samples.

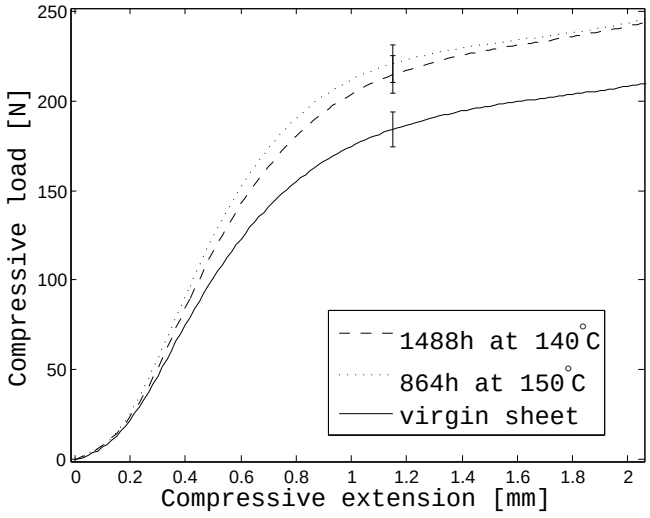

Figure 5.6: *Mean value of stress-strain graphs for indentation test performed on absorber samples from section A.*

Dimensional Changes

The results from the mapping of the dimensional changes is presented in Figure 5.7. The figure shows the width reduction in percent as a function of the exposure time at 150 °C. The error is calculated as $2\sigma_m$ where σ_m is the standard deviation of the mean calculated from the raw data in Appendix D.

Optical testing

The absorptance α of the virgin sheets, with error due to the calibration of the device, was found to be $(94.7 \pm 0.5)\%$. Figure 5.8 shows the absorptance with random error as a function of exposure temperature at 150 °C. The random error is calculated as $2\sigma_m$.

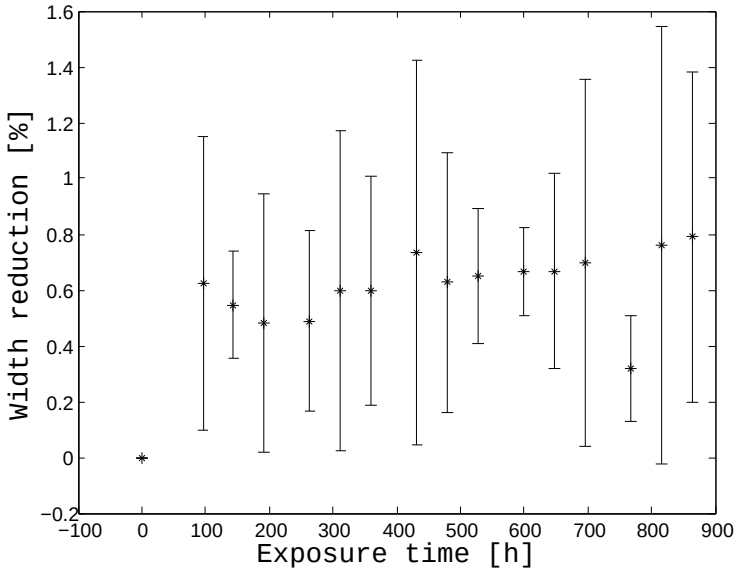

Figure 5.7: *Relative width reduction of the absorber samples as a function of exposure time at* 150 $^{\circ}C$.

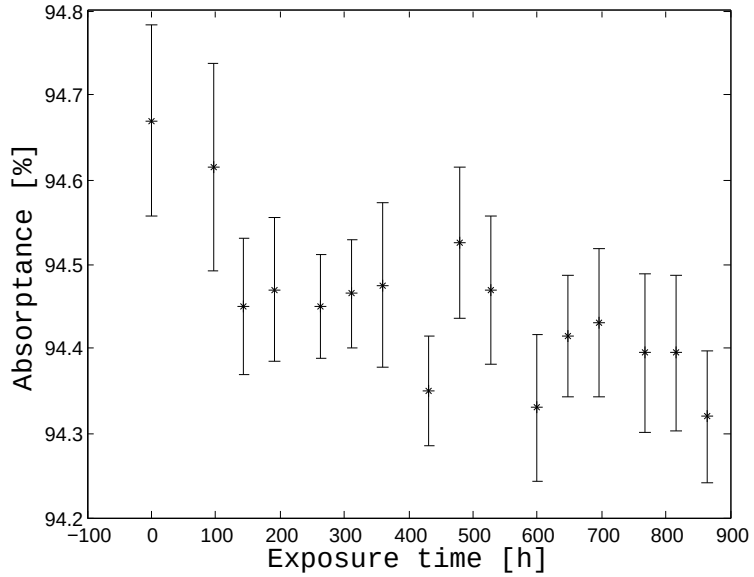

Figure 5.8: *Absorptance of the absorber samples as a function of exposure time at* 150 $^{\circ}C$.

Chapter 6

Simulation

6.1 Approach

The simulation developed in this master's thesis calculates the maximum temperatures obtainable in a Duo-Collector and investigate the performance of such a system. The terms defined below will be used in the following:

- **the glazing fraction** referres to the percentage of the absorber covered with glazing and will be denoted P. $P = 0$ corresponds to an unglazed collector, while $P = 100$ corresponds to a glazed collector.
- **the relative temperature** equals the actual temperature minus the ambient temperature.
- **the temperature rise** equals the difference between the outlet temperature and the inlet temperature.
- **the velocity** will refer to the magnitude of the velocity of the heat carrier in the upstream region of the collector.
- **the no-gain temperature** will refer to the temperature when the temperature rise equals zero.
- **the stagnation temperature** will refer to the temperature when the velocity equals zero.

Figure 6.1 shows a schematic diagram of the duo-collector. The temperatures T_i, T' and T_o represent the relative inlet temperature, the relative temperature at the border between the glazed and the unglazed region and the relative outlet temperature respectively. In the model of the system it is assumed that the heat carrier is water and that the temperature of the water in the downstream part

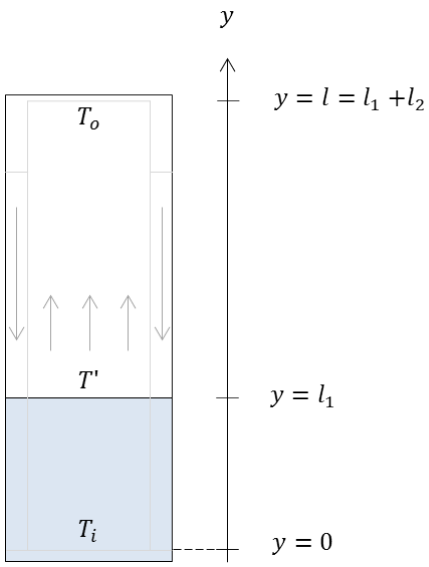

Figure 6.1: *Schematic diagram of the Duo-Collector*

of the absorber is constant. Further the model assumes steady state conditions and that the temperature in the upstream channels only changes in the y-direction.

The simulation consists of four MATLAB programs. The programs can be found in Appendix B. The following subsections present the derivations of the mathematical relations used in the simulation and descriptions of the programs. The input values used for the simulation can be seen in Table 6.1.

Derivation of temperature

In order to model the temperature change along the flow direction in the collector a volume element depicted in Figure 6.2 is considered. The arrow in the figure indicates flow direction. The heat carrier in the volume element receives an amount of energy equal $q_u dA$ per unit time. Using the relation between received heat and temperature change, $dQ = mcdT$, we find that this energy leads to a temperature increase per unit time given by

$$\frac{dT_f}{dt} = \frac{q_u dA}{mc},$$

where dA is the area of the volume element facing the sun, m is the mass of the heat carrier in the volume element and c is the specific heat capacity of the heat

Table 6.1: *Values used for simulation*

Description	Symbol	value
aperture between the innerwalls of the absorber sheet	dx	1 cm
aperture between the absorber sheet plates	dz	4 mm
height of absorber	h	3 m
ambient temperature	T_a	20 °C
absorptance of absorber sheet	α	0.947
transmittance of glazing	τ	0.84
specific heat capacity of water	c	4181 J/(kgK)
thickness of the absorber sheet plates	b	0.8 mm
density of water	ρ	1000 kg/m^3
thermal conductivity of absorber material	k	0.2 W/(mK)
back loss coefficient	U_b	1.4 W/(m^{2}K)
fraction of absorber which is glazed	P	$0 - 100\%$
radiance incident on absorber	G	$0 - 1200$ W/m^2

carrier. Using the fact that $m = \rho V = \rho dAdz$ and applying Eq. 2.1, we find that

$$\frac{dT_f}{dt} = \frac{1}{\rho c dz} F'[S - U_L(T_f - T_a)].$$

By introducing the relative temperature $T_d = T_f - T_a$, being the temperature difference between the heat carrier temperature and the ambient temperature, Eq. (6.1) gives

$$\frac{T_d}{dt} = \frac{1}{\rho c dz} F'[S - U_L T_d].$$

This is a linear differential equation leading to the following solution:

$$T_d = \frac{S}{U_L} + C_1 e^{-((F'U_L t)/(\rho c dz))},$$

where C_1 is a constant of integration.

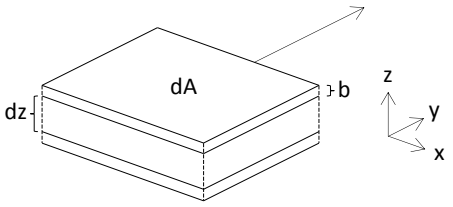

Figure 6.2: *A small volume element used for derivation of expression for the temperatures T' and T_o. The thin layers represent the two absorber plates, while the middle layer represents the heat carrier. Symbols are defined in Table 6.1.*

The glazed and unglazed regions of the duo-collector shown in Figure 6.1 need to be treated separately. The collector parameters used for the different regions can be calculated with the equations from Section 2.2 on page 7 and 8, with the values from Table 6.1. For the glazed part the water entering has the relative temperature T_i, giving the initial condition $T_d(0) = T_i$. This gives $C_1 = T_i - S/U_L$ and Eq. 6.1 becomes:

$$T' = (T_i - \frac{S}{U_L})e^{-((F'U_L t)/(\rho c dz))} + \frac{S}{U_L}, \tag{6.1}$$

where T' is the relative temperature at the border between the unglazed and glazed region and t is the time it takes the volume element to pass through the glazed region. The heat carrier entering the unglazed region has the relative temperature T', giving the initial condition $T_d(0) = T'$. This gives $C_1 = T' - S/U_L$ and Eq. 6.1 becomes

$$T_o = (T' - \frac{S}{U_L})e^{-((F'U_L t)/(\rho c dz))} + \frac{S}{U_L}, \tag{6.2}$$

where T_o is the relative temperature of the water as it leaves the absorber and enters the top of the tank and t is the time it takes the volume element to pass through the unglazed region.

The time t_i it takes for the heat carrier to pass through a regions of the absorber is given by

$$t_i = \frac{h_i}{v}$$

where h_i is the length of the region and v is the heat carrier velocity.

Derivation of velocity

A simplified model of the present absorber system which is used for the simulation is shown in Figure 6.3. The column to the left represents the downstream region,

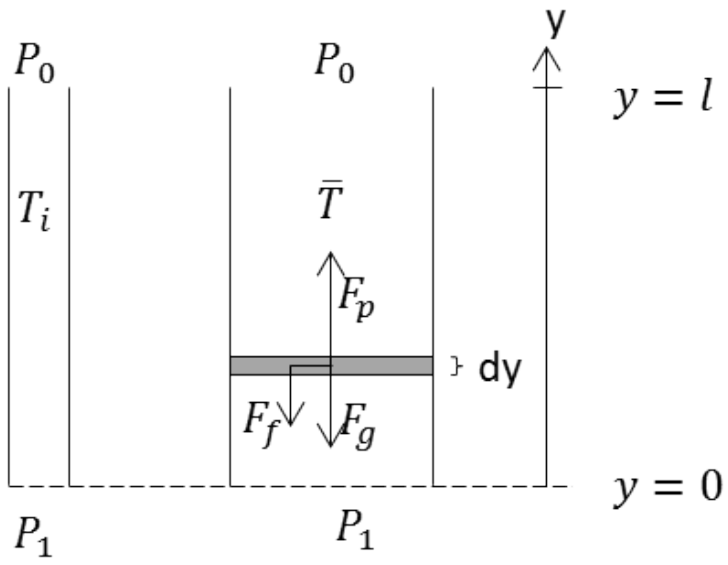

Figure 6.3: *Simplified model of duo-collector used for derivation of expression for the velocity.*

and the column to the right represents the upstream region. The pressure at the top of both columns is P_0 and the pressure at the bottom is P_1. It is assumed that the temperature distribution in the columns is homogeneous. It follows that the pressure gradient $\mathrm{d}P/\,\mathrm{d}y$ is constant. The temperature in the downstream region equals $T_i + T_a$ while the temperature used for the upstream region is the average temperature weighted with respect to the lengths h_1 and h_2, given by

$$\bar{T} - T_a = \frac{h_1\left(\frac{T_i+T'}{2}\right) + h_2\left(\frac{T'+T_o}{2}\right)}{h} = \frac{h_1 T_i + h_2 T_o + hT'}{2h}.$$

The shaded volume element in the upstream region experiences a force due to gravity, F_g, due to pressure, F_p and due to friction, F_f. Regarding forces in the y-direction as positive we have

- $F_p = (P(y) - P(y + \mathrm{d}y))\,\mathrm{d}A = -\dfrac{P(y + \mathrm{d}y) - P(y)}{\mathrm{d}y}\,\mathrm{d}V = -\dfrac{\mathrm{d}P}{\mathrm{d}y}\,\mathrm{d}V$
- $F_g = -\bar{\rho}\,\mathrm{d}V g$
- $F_f = -\mu v\,\mathrm{d}V,$

where $\bar{\rho}$ is the density of water in the upstream region, μ is a friction coefficient and v is the magnitude of the velocity in the upstream region (Grue, 2013). The

element does not experience any acceleration, hence

$$\sum F = 0 \Rightarrow \frac{\mathrm{d}P}{\mathrm{d}y} + \bar{\rho}g + \mu v = 0$$

Rearranging this equations leads us to an expression for the speed v:

$$v = -\frac{1}{\mu}\left(\frac{\mathrm{d}P}{\mathrm{d}y} + \bar{\rho}g\right). \tag{6.3}$$

Next the downstream column is used to find the pressure gradient. With the use of Eq. (2.4) on page 10 we find that

$$\frac{\mathrm{d}P}{\mathrm{d}y} = \frac{P_0 - P_1}{h} = \frac{P_0 - (P_0 + \rho_i g h))}{h} = -\rho_i g,$$

where ρ_i is the density of water at temperature $T_i + T_a$. Inserting this into Eq. 6.3 leads us to the expression for the velocity:

$$v = \frac{1}{\mu}(\rho_i - \bar{\rho})g. \tag{6.4}$$

The density of water as a function of temperature was found by fitting tabulated values (CRC Press, 2005) with a second order polynomial.

Modelling the temperature

The program temp.m found in Appendix B is used to calculate the temperature distribution in the collector. The following input parameters must be specified to run the program:

- The irradiance, G
- The glazing fraction, P
- The relative inlet temperature, T_i
- The velocity of the heat carrier , v

The other parameters needed to carry out the calculations are specified in the program and can be found in Table 6.1. The program uses Eq. 6.1 to find the temperature at the border, T', which is then used to find the outlet temperature T_o with the use of equation 6.2.

The program returns the following parameters:

- The vector T which contains the temperatures T_i, T_b and T_o
- The vector h which contains the heights h_1 and h_2 specified in Figure 6.1

For an unglazed and a glazed collector the top loss coefficients are fitted so that the relative stagnation temperatures of the systems at $G = 1000$ W/m^2 is 40 K and 120 K respectively.

Modelling the flow velocity

The function velocity.m found in Appendix B is used to calculate the heat carrier velocity. The program takes the following input parameters:

- The vector T which includes the three temperatures T_i, T_b and T_o
- The vector h which includes the two heigths h_1 and h_2

The program uses Eq. (6.4) from page 38 to calculate the velocity v. The friction coefficient μ is fitted so that heat carrier with $T_i = 0$ and $T_a = 20$°C running through a glazed collector exposed to an irradiance of 1000 W/m^2 has a temerature rise of approximately 10 K. The program returns v.

Modelling no-gain temperature

The program no_gain.m found in Appendix B calculates the no-gain temperature relative to the ambient temperature for different irradiance levels. The calculations are performed for an unglazed collector ($P = 0\%$), collectors with glazing covering 25%, 50% and 75% of the absorber and a fully glazed collector ($P = 100\%$). For a given irradiance and cover fraction, the functions temp.m and velocity.m are used in an iterative procedure. The program continues until the steady state situation when the inlet and outlet temperature are equal is reached. The no-gain temperature is defined as the temperature at the border between the glazed and the unglazed region during no-gain conditions. The no-gain temperatures for the different collectors are then presented graphically as functions of irradiance.

Modelling the efficiency

The program efficiency.m found in Appendix B produces graphs showing how the efficiency varies with the mean temperature in the collector and how the temperature rise through the collector and the velocity of the heat carrier vary with the

inlet temperature. Also, a selection of efficiencies are calculated for different outlet temperatures. All the calculations are done for $G = 1000$ W/m^2 for different glazing fraction.

To calculate the efficiency we considering a time interval t. The total useful gain during the time t can be expressed as

$$\text{Total useful gain} = vA_c\Delta Tct/\rho.$$

ΔT is the temperature rise through the collector given by $T_o - T_i$ and A_c is the cross section of the upstream channels perpendicular to the flow direction. The solar energy received is given by

$$\text{Solar energy received} = AGt,$$

where A is the area receiving solar energy. In the calculations presented here the area A is defined as the contact area between the heat carrier and the top plate. By employing Eq. (2.2) on page 8 we find that the efficiency is given by

$$\eta = \frac{vA_c\Delta Tc}{\rho AG}.$$

6.2 Results

The fitting of the parameters U_t and μ can be found in Table 6.2. Figure 6.4 shows the no-gain temperature above ambient temperature as a function of irradiance for collectors with different glazing fractions. Figure 6.5 shows the efficiency of collectors with different glazing fractions as a function of the relative mean heat carrier temperature. The efficiency for some outlet temperatures and glazing fractions are presented in Table 6.3. The temperature rise and the velocity of the heat carrier as a function of the inlet temperature can be seen in Figures 6.6 and 6.7. All the results are calculated with $T_a = 20$ °C.

Table 6.2: *Collector parameters fitted to the simulation.*

U_t (glazed)	5.3 W/(m^{2}K)
U_t (unglazed	22 W/(m^{2}K)
μ	900 kg/(m^{3}s)

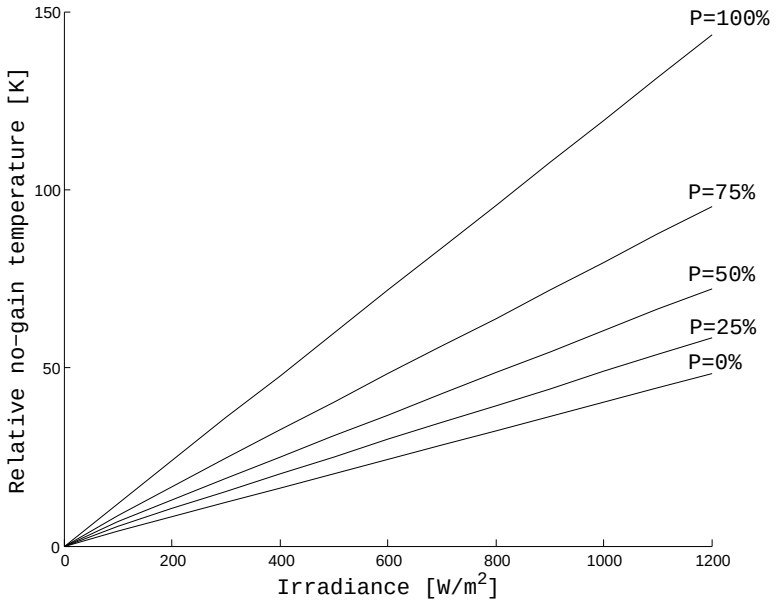

Figure 6.4: *No-gain temperature as a function of irradiance for different glazing fractions P.*

Table 6.3: *Efficiencies [%] for different outlet temperatures T_o and glazing fractions P ($G = 1000\ W/m^2$).*

	$T_o = 10$ °C	$T_o = 20$ °C	$T_o = 30$ °C	$T_o = 40$ °C	$T_o = 50$ °C
$P = 50\%$	74	58	43	27	11
$P = 75\%$	74	63	52	41	30
$P = 100\%$	75	68	61	55	48

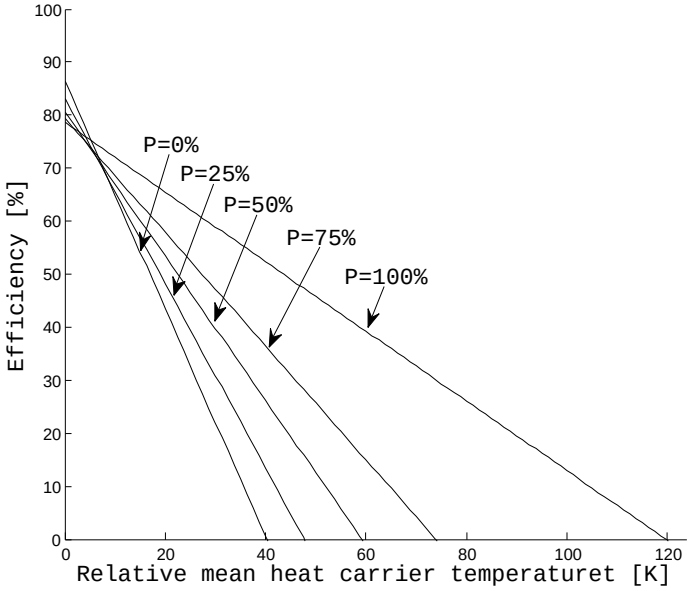

Figure 6.5: *Efficiency as a function or the relative mean heat carrier temperature for different glazing fractions P ($G = 1000\ W/m^2$).*

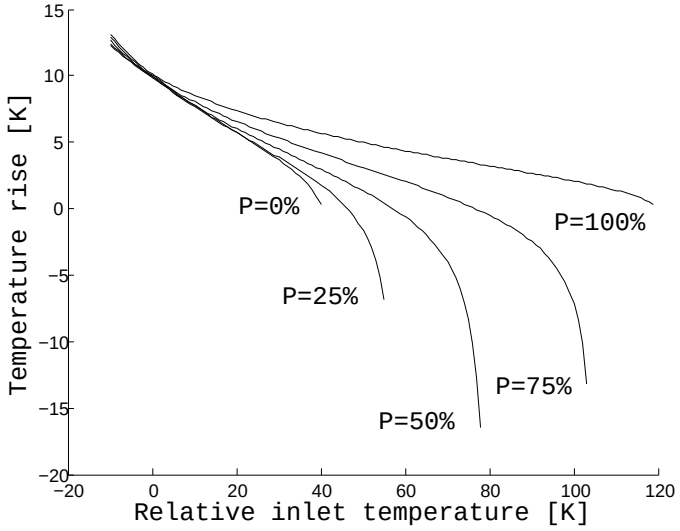

Figure 6.6: *Temperature rise as a function of relative inlet temperature for different glazing fractions P ($G = 1000\ W/m^2$).*

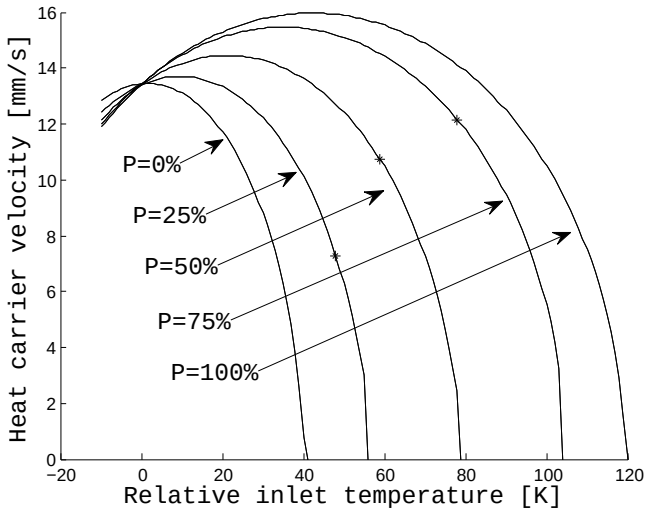

Figure 6.7: *Heat carrier velocity as a function of inlet temperature for different glazing fractions P ($G = 1000\ W/m^2$). The asterisks (*) indicate no-gain velocities.*

Chapter 7

Discussion

7.1 Discussion of experimental results

Indentation tests

Initially the plan was to analyze the changes in the mechanical properties of the absorber by the use of indentation tests for three different heat ageing temperatures. As polypropylene generally is expected to be less resistant to thermal load compared to engineering thermoplastics and high performance polymers (see Figure 3.1) it was expected that changes would occur in a relatively short time period, allowing us to conduct the experiment during the available time forseen for the present thesis using one heating cabinet. Before the wellshaped specimens were available, some misshaped specimens were exposed to heat ageing at 120 °C. As none of the specimens reached failure during indentation tests after an exposure time of approximately a week it was decided to use two heating cabinets and start heat ageing at 120 °C and 140 °C as soon as the wellshaped specimens were available. Since the heat ageing at 140 °C did not lead to any measurable results during the first four weeks it was decided to end the heat ageing at 120 °C in order to increase the temperature further. The indentation tests presented in this work were conducted on specimens which received thermal load at 140 °C and 150 °C. None of the specimens reached the fracture point during testing. Increased exposure temperatures and/ or exposure times should be applied if the experiment is to be repeated.

Figure 5.3 on page 28 shows how the specimens fold during testing, so that an angle is created between the specimen and the supporting surface. It would be of interest to investigate the behavior of indentation tests performed in such a way that the specimens are prevented from folding. It is reasonable to assume that if the specimens are prevented form folding, the force applied on the top plate will

be greater for the same indentation depth, which might lead to results earlier than with the given method. Unfortunately it was not possible to investigate this due to lack of time.

The stress-strain diagrams in Appendix C suggests that the results from the indentation test performed on specimens from section A are less spread out than the results corresponding to section B. This might be due to variations in the geometry of the sheet. The different sections of the sheet experience slightly different conditions during the extrusion process. This might also cause differences in the mechanical properties. Figures 5.5 and 5.6 are produced from results from indentation tests from section A.

From Figure 5.6 it can be seen that the very first part of the curve has an increasing slope. It is not clear why the behavior is non-linear in the beginning. This behavior is observed for compressive extension between 0 and approximately 0.2 mm. One explanation might be that a certain compression is necessary for the specimen to obtain total contact with the supporting surface and the indenter, due to small variations in the geometry. The next part of the curve shows a linear behavior. Compared to the virgin sheets the thermally treated sheets need slightly larger load to reach the same indentation depth. The increase of the slope represents an increase of the stiffness of the samples, as described in Section 3.2. Hence it can be concluded that the heat ageing has increased the stiffness of the specimens.

When the compressive extension reaches approximately 1.2 mm the elastic limit is reached and the compression is of plastic behavior. The last part of the curve in Figure 5.5 represents the behavior after the two plates come in contact. The two plates are compressed together and the deformation only occurs in the material, in contrast to the earlier stages when the compression also occurred in the air gap between the plates. In this region a large load is needed for a small deformation. The fracture of the specimens was expected to occur after the elastic limit and before the plates came in contact.

Figure A.1 on page 62 shows the surface of an absorber sample made of a polypropylene material which has been exposed to heat ageing at 130 °C for 115 hours. The damage of the surface is clearly visible. There were no visible changes of the specimens used in the current experiment despite of the fact that the exposure time was longer and the temperature was higher. This illustrates that the results deviate strongly from first expectations.

Da Silva (2008) investigated how results of the indentation tests depend on the width of the tested specimens. The results presented in Figure A.3 are from indentation tests on virgin specimens made of PPS. They show that the slope of the linear region increases with increasing width. Comparing the curve corresponding to tests done on specimens with a width of 48 mm and performed on the top surface with the solid line in Figure 5.6 we see that for indentation depths of 0.5 mm the loads are approximately 140 N and 100 N respectively. Hence the slope of the indentation curves of the PP absorber is slightly smaller. Taking into account that da Silva's specimens are slightly wider we can conclude that the stiffness of the PP absorber tested in this work and the PPS absorber tested by da Silva are of similar size.

Figure A.2 shows the result from indentation tests performed on a PPE/PS blend. These can be found in the bottom and middle left cells in the pyramid shown in Figure 3.1 on page 16. The width of the specimens tested were from $72 - 87$ mm. Compared to the results of samples with a width of 81 mm from Figure A.3 we see that the stiffness of the PPE/PS specimens is larger than that of the PPS. The increased stiffness leads to a larger indentation load during the region where fracture is expected to occur. Stiffness depends on the shape as well as the material. Since the absorber sheet made of the PPE/PS material was a triple-wall sheet we cannot draw conclusions about the stiffness of the materials relative to each other. This shows that the design parameters are of great importance for the results of indentation tests.

The absorber samples made of the material BA160E clearly withstands exposure to dry heat load better than expected from previous studies om PP materials. It would be intersting to compare to which extent the present PP specimens can sustain dry heat ageing in comparison to PPS specimens. Further investigations are needed to give quantitative results.

Dimensional changes

The mapping of the dimensional changes was done on the absorber samples which were exposed to heat ageing at 150 °C. The reduction in width for the different exposure times are presented in Figure 5.7. The measuring point corresponding to an exposure time of 768 h clearly stands out. In the raw data presented in Appendix D it can be seen that the difference in the width on location e for the given exposure time is the only negative value, which corresponds to an increase of the width as a result of the heat ageing. A total of 180 measurements were performed to produce the raw data. It is likely that this is a measurement error. The first point in Figure 5.7 is not a measurement point. As this point represents

the reduction in width for a virgin absorber it must be zero to make physical sense.

Although the measurement points do not give a clear correlation between the exposure time and the reduction in width they indicate that the reduction mainly occurs in the early stages of the heat exposure. According to the theory presented in Section 3.3 physical ageing due to molecular relaxations lead to a reduction of the materials volume. Since the molecular relaxation gradually draws the material closer to equilibrium the rate is expected to be degressive (decrease with time) leading to a more significant change in the beginning. This is in agreement with the measured results as the difference between the first and the second point in Figure 5.7 is large compaired to the the difference between the rest of the points. This behavior also suggests that most of the reduction has occurred within the early stages of the heat ageing. By decreasing the time interval between the measurement points, especially in the region between 0 and 96 hours, the behavior could be mapped with greater detail.

The cause of the errors might be local variations both in the composition of the material and the geometry. The reduction is measured to be less than 1%. As the expected value was between 1% and 2% this is a satisfying result.

Optical testing

The absorptance as a function of exposure time at 150 °C is shown in Figure 5.8. As the aim was to study the change in absorptance of the absorber the systematic error caused by the calibration of the alphameter is not included in the figure. This error is much larger than the errors presented in the figure and it is important to include the calibration error when considering the certainty of the measured values in comparison to other material surfaces. The samples used for the current experiment were also used for mapping the dimensional changes, and some were also used to perform indentation tests. The handling of the samples might have affected the results, for example by causing the surface to be scratches or soiled.

The results show a decrease in the absorptance as a function of exposure time. The exposure times were up to about five weeks, and during this time the reduction in absorptance was less than 0.4%. The values presented in Table A.1 in Appendix A show absorptance measurements performed on PPS absorber samples. The values are presented for different wavelengths. All the values are below the measured absorptance of the material tested in the current work, which was $(94.7 \pm 0.5)\%$. Since the solar energy absorbed by a flat plate collector is proportional to the absorptance it is preferrable with high absorptance values. The absorptance of the surface of the absorber shows satisfying absorptance properties for solar thermal

applications.

7.2 Discussion of results from simulation

The simulation programs developed were fitted to fit the empirical behavior of unglazed and glazed collectors. Still, the program is based on a number of assumptions. It is therefore important to emphasize that the results produced by the programs might deviate from the actual behavior of a Duo-Collector. The model should be compared with empirical behavior to be verified.

No-gain temperature

The no-gain temperature as a function of irradiance for collectors with different glazing fractions is presented in Figure 6.4. The figure shows that there is not a linear relation between the glazing fraction and the no-gain temperature; a collector with a glazing fraction of 50% has a no-gain temperature which lies closer to the stagnation temperature of an unglazed collector than to that of a glazed collector. An interpretation of this can be found by looking at the mathematical basis of the simulation. Let T_g and T_u be the stagnation temperatures for a glazed and an unglazed collector respectively and consider a collector with glazing fraction equal 50%. Next we let the mean heat carrier temperature in this collector be $(T_g + T_u)/2$. The absorbed energy is not affected by the temperature change of the fluid. This means that the absorbed energy equals the sum of the absorbed energy for the two different regions. The heat loss on the other hand depends on the temperature difference between the mean heat carrier temperature and the ambient. The loss from the unglazed region of the Duo-Collector will therefore be larger than the loss from an unglazed collector during no-gain conditions. Similarly, the heat loss from the glazed region of the partially covered collector will be smaller than the loss from a glazed collector at stagnation. If the reduction in heat loss was to compensate the increase in heat loss $(T_g + T_u)/2$ would be the no-gain temperature since the net energy budget would be zero. This is not the case because the heat loss coefficient for the unglazed part is larger than that of the glazed part. This results in a situation where the energy loss exceeds the energy absorption. Hence the temperature of the heat carrier will be reduced, and approach a temperature which lies closer to T_u.

The Duo-Collector design is meant to prevent overheating. A well dimensioned system is not expected to reach boiling temperatures during normal application. The results from the simulation shows that during periods of time when hot water

is not drawn from the tank the temperature in the Duo-Collector will be limited by the no-gain temperature for the given conditions.

Performance

The efficiency for different glazing fractions can be seen in Figure 6.5. The figure shows that the difference in efficiency for the different collectors increases with increasing operating temperatures. The calculated values corresponding to relative mean heat carrier temperatures equal to zero are found where the efficiency curves intersect the y-axis. This gives a total heat loss equal zero. The efficiencies obtained when there is no heat loss are proportional to the absorbed solar energy. The unglazed collector has the largest efficiency at this point due to the large absorptance.

The temperature rise and the velocity of the heat carrier are presented as functions of the inlet temperature in Figures 6.6 and 6.7. The efficiency is proportional to the product of the temperature rise through the collector and the velocity of the heat carrier. Since the efficiency decreases with increasing inlet temperature, the product of these two graphs must also decrease. If we consider the behavior of a fully glazed collector we find that for inlet temperatures below approximately 50 °C the velocity increases with increasing inlet temperatures. The efficiency decrease for this region is therefore solely due to a reduction in the temperature rise. For larger inlet temperatures the decrease is due to a reduction of the velocity as well as the temperature. A similar behavior is observed for all graphs, but the maximum velocity is found at different temperatures for the different collectors.

Comparing Figures 6.6 and 6.7 for collectors with glazing fractions of $P = 0\%$ and $P = 100\%$ it can be seen that the inlet temperature which gives a zero temperature rise corresponds to a velocity equal to zero. For the Duo-Collectors the heat carrier velocities corresponding to $T_o - T_i = 0$ is not zero. The asterisks in Figure 6.7 indicate the velocity during no-gain conditions. The velocity of the heat carrier during no-gain conditions is not zero for a Duo-Collector. The term *stagnation temperature* has therefore been avoided when discussing the Duo-Collector. The reason why the heat carrier circulates during no-gain conditions is that the temperature at the border between the glazed and unglazed region is higher than the inlet and outlet temperature. This results in a mean density in the upstream region, $\bar{\rho}$, smaller than the density in the downstream region, ρ_0. From Eq. (6.4) we see that this density difference gives rise to the circulation, and therefore the Duo-Collector maintains circulation.

The figures show that for a Duo-Collector the temperature rise of the heat carrier

can take negative values for positive velocities. If the inlet temperature exceeds the no-load temperature, for example after a decrease in the irradiance, the collector can continue to circulate, cooling the heat carrier letting it approaches the no-load temperature. For given ambient conditions this process applies for a limited temperature region. The velocity during the cooling is limited by the velocity during no-gain conditions. It is not clear if this effect will be negligible or of great influence, and further investigations are needed in order to analyze this.

Table 6.3 shows a selection of calculated efficiencies. The performance of the Duo-Collector is approximately equal to that of a glazed collector for low relative outlet temperatures. The efficiency decreases with increasing outlet temperatures. If the desired temperature in the tank is 70 °C and the ambient temperature is 20 °C the region of interest is for relative outlet temperatures up to 50 °C. For relative outlet temperature equal 40 °C, corresponding to an actual outlet temperature of 60 °C, the efficiency for the collector with $P = 50\%$ is is close to 30%, approximately half the value of the efficiency of a glazed collector. For relative outlet temperature equal 50 °C, corresponding to an actual outlet temperature of 70 °C, the efficiency of the collector with $P = 50\%$ has dropped to around 10%.

Chapter 8

Summary

The absorber samples extruded from polypropylene BA160E has shown high sustainable to thermal load compared to what is expected from polypropylene components. The absorber samples also show good dimensional stability. During 864 hours at 150 °C the relative width reduction was measured to be $< 1\%$. The absorptance was measured to be $(94.7 \pm 0.5)\%$, with a reduction of less than 0.4% during the heat exposure. Initially the plan was to measure the emittance of the absorber as well. Unfortunately the required equipment was not available. The results indicate that the tested absorber sheet is a good candidate for use in flat plate collectors. As the price of the tested polypropylene material is lower than that of the PPS material currently used in the AventaSolar collectors it would be of interest to compare the two, but this requires further investigations.

The simulation of the Duo-Collector suggests that the design works well as a method to prevent boiling of the heat carrier. The program predicts how the glazing fraction affects the maximum temperature for given ambient conditions. The efficiency of a collector with a glazing fraction of 50% is similar to that of a glazed collector for low inlet temperatures. The efficiency of the Duo-Collector decreases more rapidly when the operating temperatures increase. The results presented were produced with an ambient temperature or 20 °C and an irradiance of $1000\mathrm{W/m^2}$. For relative outlet temperatures of 40 °C, corresponding to an actual temperature of 60 °C, the efficiency of the Duo-Collector was calculated to be 27%.

In contrast to the fully glazed or unglazed collectors, the Duo-Collectors can, during certain circumstances, cool the water even though the velocity of the heat carrier is positive. This mechanism should be investigated further in order to find out if this can be avoided. Analysis of performance of fully glazed and partially glazed collectors for different regions and purposes are not discussed in this work, but could be a topic for further research.

The combination of the tested absorber sheet and the Duo-Collector has the potential to reduce the cost and increase the reliability of solar water heaters further. Hopfully the research on low cost solar water heaters can contribute so that utilization of solar thermal power can increase even faster in the years to come.

References

Alghoul, M., Sulaiman, M., & Azmi, B. (2005). Review of materials for solar thermal collectors. *ANTI-CORROSION METHODS AND MATERIALS 4*, *52*, 199-206.

Bockhorn, H., Hornung, A., Hornung, U., & Schawaller, D. (1999). Kinetic study on the thermal degradation of polypropylene and polyethylene. *Journal of Analytical and Applied Pyrolysis*, *48*, 93-109.

Borealis. (2013). *personal communication.*

Chaurasia, P. (2000). Solar water heaters based on concrete collectors. *Energy*, *25*, 703-716.

CRC Press. (2005). *Handbook of Chemistry and Physics, Internet version.* Retrieved from `http://www.hbcpnetbase.com` (Accessed: 2013-05-22)

da Silva, L. C. (2008). *New generation of solar thermal collectors.*

Duffie, J. A., & Beckman, W. A. (2006). *Solar engineering of thermal processes* (3. ed.). Wiley.

Grue, J. (2013). *personal communication.*

HTCO GmbH. (2012). *Cfd simulation tss-aventa* (Tech. Rep.).

IPCC. (2007). *Fourth assessment report of the intergovernmental panel on climate change.*

Kahlen, S., Wallner, G., & Lang, R. (2010a). Aging behavior of polymeric solar absorber materials - part 1: Engineering plastics. *Solar Energy*, *84*, 1567-1576.

Kahlen, S., Wallner, G., & Lang, R. (2010b). Aging behavior of polymeric solar absorber materials - part 2: Commodity plastics. *Solar Energy*, *84*, 1577-1586.

Kim, J., Lee, W. I., & Tsai, S. W. (2002). Modeling of mechanical property degradation by short-term aging at high temperatures. *Composites: Part B*, *33*, 531-543.

Meir, M. (2013). *Personal communication.*

Metiu, H. (2006). *Physical chemistry kinetics.* Taylor & Francis Group.

Morrison, G. L. (2001). Solar collectors. In J. Gordon (Ed.), . James & James Ltd.

Olivares, A. (2008). *Service life estimation for a polymeric solar absorber.* Unpublished doctoral dissertation, University of Oslo.

Olivares, A., Rekstad, J., Meir, M., Kahlen, S., & Wallner, G. (2008). A test procedure for extruded polymeric solar thermal absorbers. *Solar Energy Materials & Solar Cells*, *92*, 445-452.

Olivares, A., Rekstad, J., Meir, M., Kahlen, S., & Wallner, G. (2010). Degradation model for an extruded polymeric solar thermal absorber. *Solar Energy Materials & Solar Cells*, *94*, 1031-1037.

Optosol. (n.d.). Retrieved from `http://www.optosol.com` (Accessed: 2013-05-24)

Optosol. (2002). [Computer software manual].

Plastics Europe Market Research Group. (2011).

Rekstad, J. (2007). *Polymers from a market perspective ideas for future development* (Tech. Rep.). IEA Solar Heating & Cooling Programme.

Rekstad, J. (2013). *personal communication.*

Rekstad, J., & Meir, M. (2010). Solar collector absorbers in high-performance polymeric materials. *EuroSun 2010, International Conferance on Solar Heating, Cooling and Buildings*, Graz, Austria.

Rekstad, J., & Meir, M. (2012). *Energy an physics - compendium for FYS4540/9540: Energy Physics - Solar Energy.*

REN21. (2012). *Renewables 2012: Global status report* (Tech. Rep.).

Resch, K., & Wallner, G. M. (2012). Plastics market. In *Polymeric materials for solar thermal applications* (chap. 7). Wiley-VCH.

Siqueira, D., Vieira, L., & Damasceno, J. (2011). Analysis and performance of a low-cost solar heater. *Renewable Energy*, *36*, 2538-2546.

Statistisk Sentralbyrå. (2013). *Utslipp av klimagasser, 1990-2011, endelige tall.*

Termaks. (2013). *Technical spesifications laboratory drying ovens - sterilizers.* Retrieved from `www.termaks.com` (Accessed: 2013-05-22)

Tsilingiris, P. (1999). Towards making solar water heating technology feasiblethe polymer solar collector approach. *Energy Conversion and Management*, *40*(12), 1237 - 1250.

Tsilingiris, P. (2002). Back absorbing parallel plate polymer absorbers in solar collector design. *Energy Conversion and Management*, *43*(1), 135 - 150.

Wallner, G. M., Lang, R. W., & Schnetzinger, K. (2012). Polymeric materials. In *Polymeric materials for solar thermal applications* (chap. 8). Wiley-VCH.

Weiss, W., & Mauthner, F. (2012). *Solar heat worldwide* (Tech. Rep.). IEA Solar Heating & Cooling Programme.

White, J. R. (2006). Polymer ageing: physics, chemistry or engineering? Time to reflect. *Comptes Rendus Chimie*, *9*(1112), 1396 - 1408.

Young, H. D., & Freedman, R. A. (2004). *University physics with modern physics* (11. ed.). Addison Wesley.

Appendices

Appendix A

Results from earlier studies

Figure A.1 shows the surface of a polypropylene material which has been exposed to 130 °C for 115 hours (Olivares, 2008). Figure A.2 shows a stress-strain diagram from a triple-wall sheet made of a PPE/PS blend (Olivares et al., 2008). The exposure temperature was 120 °C, and the different exposure times can be found in the figure. Figures A.3 and A.4 shows the results from investigations done by da Silva (2008). The stress-strain curves for tests done on specimens with different widths (Figure A.3) and on different exposure times (Figure A.4) at 150 °C are presented in the figures. The measured absorptance of the PPS material tested by da Silva (2008) are presented in Figure A.1.

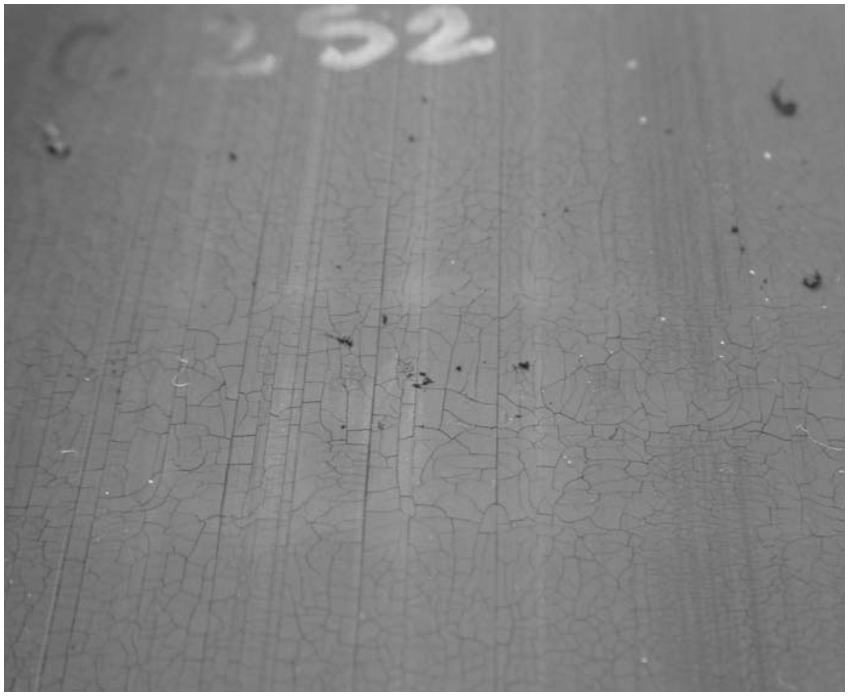

Figure A.1: *Polypropylene specimen exposed to* 130 °*C for* 115 *hours.*

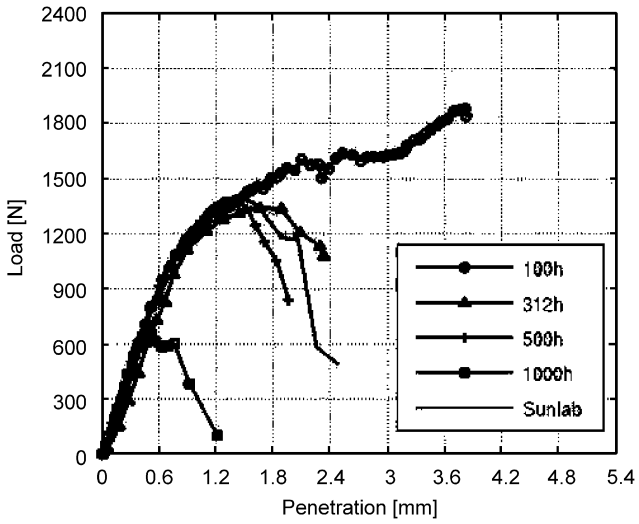

Figure A.2: *Results from indentation tests performed on triple-wall sheet made of a PPE/PS blend exposed to* 120 °*C.*

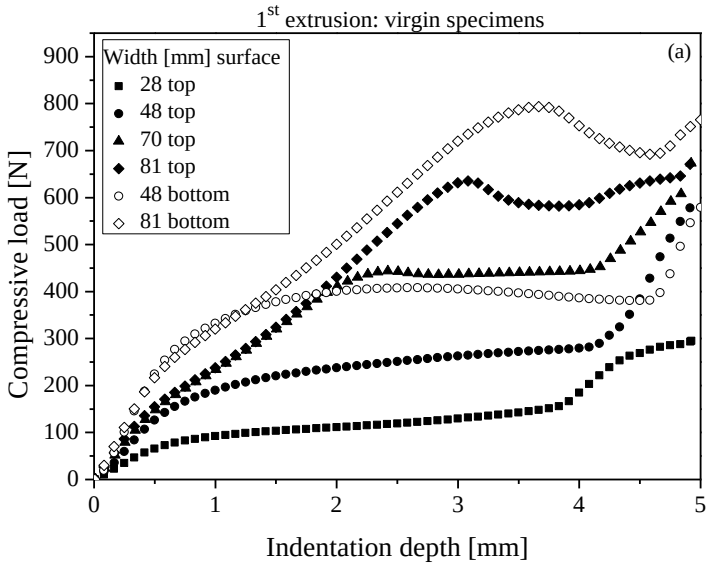

Figure A.3: *Results from indentation tests performed on virgin specimens with different widths.*

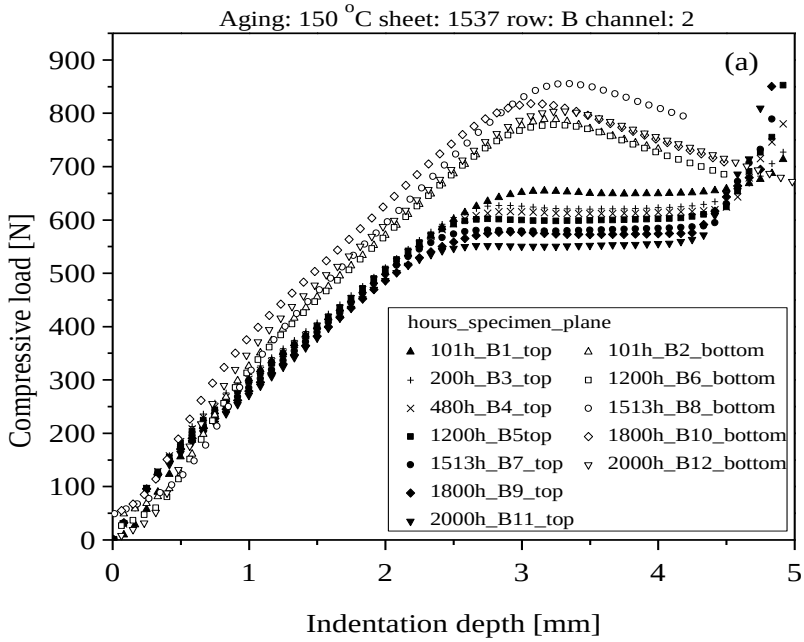

Figure A.4: *Results from indentation tests performed on twin-wall sheet made of PPS.*

Table A.1: *Absorptance measurements for different exposure times performed on the PPS material.*

	Average absorptance in [%] of PPS based alloy				
150 °C	Wavelength, λ [nm]				
1st extrusion	470 (Blue)	570 (Green)	640 (Red)	895 (IR)	1300 (W halogen)
0h	88.7±0.1	89.7±0.2	90.3±0.1	90.7±0.1	90.7±0.1
28 h	88.6±0.1	89.8±0.1	90.2±0.2	90.6±0.1	90.3±0.1
101 h	88.6±0.1	89.7±0.1	90.1±0.1	90.4±0.1	90.4±0.1
200 h	88.7±0.1	90.2±0.2	90.4±0.2	90.6±0.2	90.4±0.1
480 h	88.5±0.1	89.4±0.1	89.8±0.1	90.3±0.1	90.3±0.1
1200 h	88.8±0.1	89.9±0.1	90.0±0.1	90.5±0.1	90.5±0.1
1513 h	89.3±0.1	89.9±0.1	90.2±0.1	90.7±0.1	90.1±0.1
1800 h	89.5±0.1	90.0±0.1	90.4±0.1	90.7±0.1	91.0±0.1
2000 h	89.3±0.1	89.9±0.1	90.5±0.1	90.7±0.1	90.8±0.1
200 °C					
1st extrusion					
2nd extrusion					
0h	-	-	-	-	-
	89.3±0.1	90.2±0.2	90.3±0.2	90.9±0.2	90.4±0.1
20h	89.4±0.1	90.1±0.1	90.5±0.1	90.7±0.1	90.7±0.1
	89.4±0.1	90.3±0.1	90.2±0.1	90.6±0.1	90.3±0.1
50h	89.1±0.1	90.1±0.1	90.3±0.1	90.4±0.1	90.4±0.1
	89.6+0.1	90.3±0.1	90.2±0.1	90.7±0.1	90.4±0.1
100h	89.3±0.1	90.2±0.1	90.5±0.1	90.5±0.1	90.6±0.1
	90.2±0.1	90.8±0.1	90.7±0.1	91.1±0.1	90.9±0.1

Appendix B

MATLAB scripts

Temp.m

```
function [T, l] = temp(I, P, T_i, v_2)
dz=4e-3; %aperture between plates [m]
v_2=v_2*1e-3;
l=3;
U_b=0.035/25e-3; %W/(m^2K)
U_t=[5.3 22];
alpha = 0.947;
tau = 0.84;
c=4181; % spesific heat capacity of water J/(kgK)
b=8e-4; %thickness of polymer plates
rho=1000; %kg/m^3
k=0.2; %0.1-0.22 thermal conductivity polymers

l_1=P*l/100;%length of glazed part
l_2=l-l_1;%length of unglazed part
l=[l_1 l_2];
H=k/b;
S=[I*alpha*tau*1.01 I*alpha];
t_1=l_1/v_2; %time spent in glazed part downstream
t_2=l_2/v_2; %time spent in unglazed part downstream
t = [0 t_1 t_2];
T=ones(1,3);
T(1)=T_i;

U_L=U_t.*(1+1/(1+H/U_b))+U_b*(1-1/(1+H/U_b));
F=1./(1+U_t./H);
K_1=F.*U_L./(rho*c*dz);
for j=1:2
    T(j+1)=(T(j)-S(j)/U_L(j))*exp(-K_1(j)*t(j+1))+S(j)/U_L(j);
end
```

velocity.m

```
function [v] = velocity(T, l)
T_a=20;
T=T+T_a;
g=9.81;
mu=900;
rho_0= 1000.5-0.0695*T(1)-0.0036*T(1)^2;
T_bar = (l(1)*(T(1)+T(2))/2 + l(2)*(T(2)+T(3))/2)/sum(l);
rho_bar=1000.5-0.0695*T_bar-0.0036*T_bar^2;
v=1/mu*(rho_0-rho_bar)*g*1e3;
end
```

no_gain.m

```
close all;
clear all;
accuracy = 0.000001;
I=linspace(0, 1200, 25);
percent_glazed = [0 25 50 75 100];
T_s=zeros(length(I), length(percent_glazed));
T=[];
for i=1:length(I)
    for j=1:length(percent_glazed)
        T(3)=0;
        T(1)=3;
        v=2;
        while abs(T(3)-T(1)) > accuracy
            [T, l]=temp(I(i), percent_glazed(j), T(3), v)
            v = velocity(T, l)
        end
        T_s(i, j)= T(2);
    end
end
figure(1)
hold on
for i=1:length(percent_glazed)
plot(I, T_s(:,i), 'k')
end
xlabel('Irradiance')
ylabel('Relative no-gain temperature')
hold off
```

efficiency.m

```
clear all;
close all;
accuracy = 0.000001;
l=3;
dz=4e-3; %aperture between plates [m]
dx=1e-2;
A=l*45*dx;
T_a=20;
T_i=linspace(-10, 180, 191);
c=4181;
cross_section = 45*dx*dz;
P=[0 25 50 75 100];
l_1=P*l/100;%length of glazed part
l_2=l-l_1;%length of unglazed part
l=[l_1 l_2];
I=1000;
color='rgckb';
eff=zeros(length(P), length(T_i));
temperature_out=zeros(length(P), length(T_i));
speed=zeros(length(P), length(T_i));
iterative=zeros(length(P), length(T_i));
barT=zeros(length(P), length(T_i));
marks=zeros(1, length(P));
for i=1:length(P)
    for j=1:length(T_i)
        T=[0 0 0];
        v=1;
        dummy = T(3)+1;
        dummy_v=v;
        while abs(dummy - T(3)) > accuracy
            v=(dummy_v+v)/2;
            dummy_v=v;
            dummy = T(3);
            iterative(i,j) = iterative(i,j) + 1;
            [T, l]=temp(I, P(i), T_i(j), v);
            v=velocity(T, l);
            if v<0
                v=0;
                T(3)=T_i(j);
                dummy = T(3);
            end

        end
        eff(i,j)=(T(3)-T(1))*v*cross_section*c/(I*A);
        speed(i, j) = v;
        barT(i,j)=(l(1)*(T(1)+T(2))/2 + l(2)*(T(2)+T(3))/2)/sum(l);
        temperature_out(i,j)=T(3);
```

```
48      end
49  end
50  figure(5)
51  box on
52  axis([0 130 0 100])
53  xlabel('Mean heat carrier temperature above ambient [^\circC]')
54  ylabel('Efficiency [%]')
55  hold on
56  for i=1:length(P)
57      Eff=eff(i,:);
58      Eff(Eff<=0)=[];
59      BarT=barT(i,1:length(Eff));
60      p=polyfit(BarT, Eff, 1);
61      marks(i)=-p(2)/p(1);
62      x=linspace(0, 130, 100);
63      plot(x, 100.*(p(1).*x+p(2)), 'k')
64      p = polyfit(temperature_out(i,1:length(Eff)), Eff, 1);
65      x=linspace(10, 50, 5);
66      E=p(1).*x+p(2)
67  end
68  marks=round(marks);
69  figure(1)
70  hold on
71  figure(2)
72  hold on
73  for i=1:length(P) %Produces temp rise and velocity
74      V=speed(i,:);                %as functions of inlet temp.
75      V(V==0)=[];
76      X=length(V)+1;
77      figure(1)
78      plot(T_i(1:X), [V 0], 'k');
79      figure(2)
80      plot(T_i(1:X-1), temperature_out(i,(1:X-1))-T_i(1:X-1), 'k');
81      if i==2 || i==3 || i==4
82      j=V(T_i==marks(i));
83      figure(1)
84      plot(marks(i), j, 'k*')
85      end
86  end
87  hold off
```

Appendix C

Indentation tests

Figures C.1-C.3 show the results from the indentation tests on virgin specimens, specimens exposed to 140 °C for 1488 h and specimens exposed to 150 °C for 864 h.

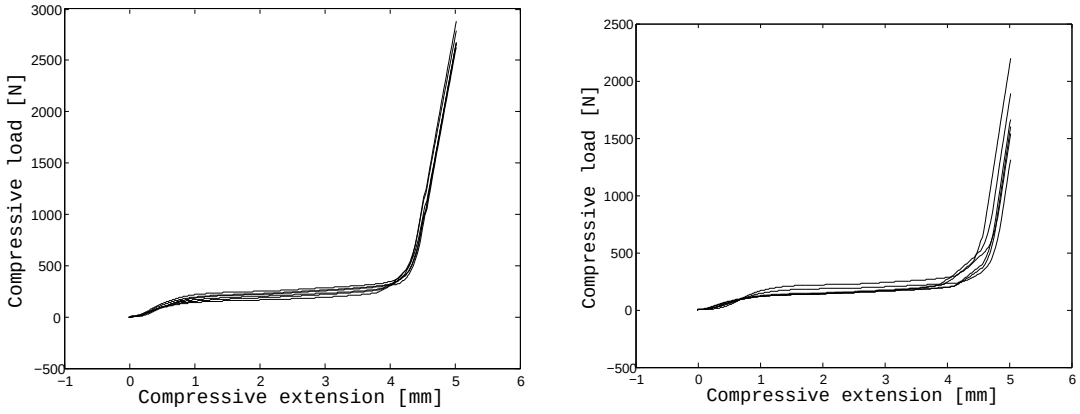

(a) Specimen from section A **(b)** Specimen from section B

Figure C.1: *Results from indentation test for virgin specimens.*

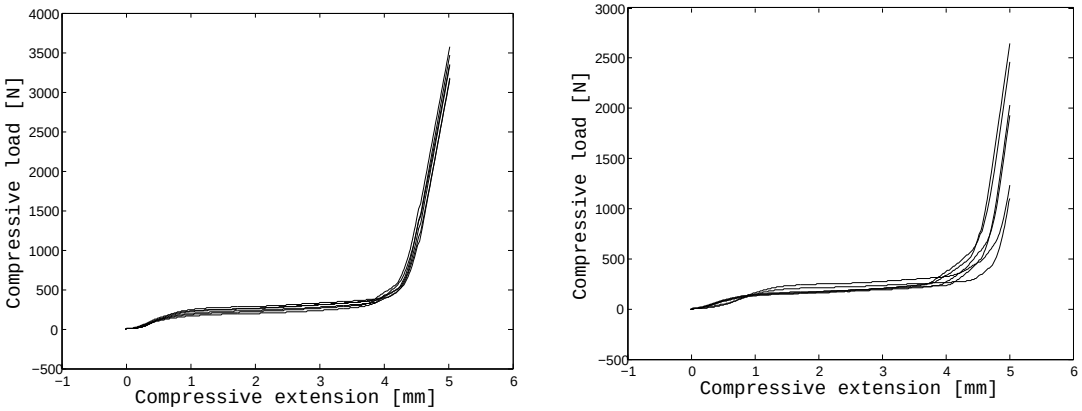

(a) Specimen from section A **(b)** Specimen from section B

Figure C.2: *Results from indentation test for specimens exposed to* 140 $^{\circ}C$ *for* 1488 *h.*

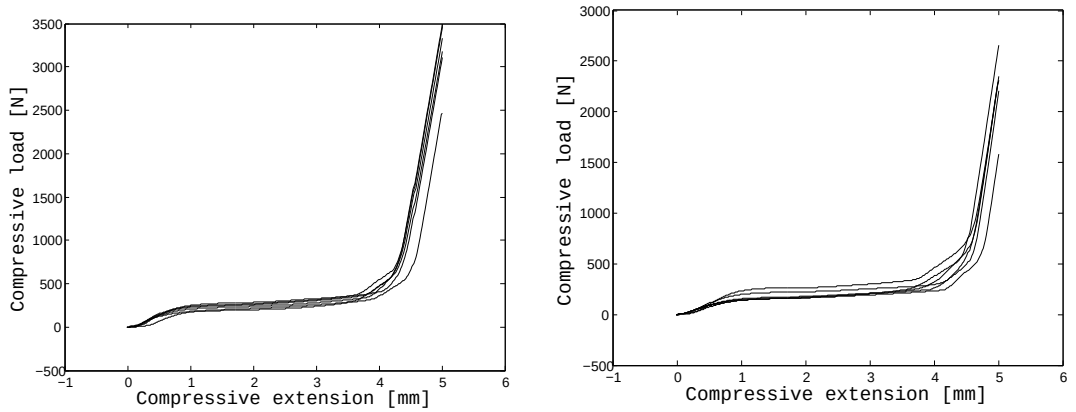

(a) Specimen from section A **(b)** Specimen from section B

Figure C.3: *Results from indentation test for specimens exposed to* 150 $^{\circ}C$ *for* 864 *h.*

Appendix D

Raw data: dimensions

The values listed below give the relative width reduction for specimens exposed to 150 °C. The letters a-f correspond to different measuring positions and the exposure times are found to the right.

a	b	c	d	e	f		
0.0101	0.0080	0.0060	0.0051	0.0041	0.0041	96	hours
0.0070	0.0045	0.0030	0.0050	0.0056	0.0076	144	hours
0.0096	0.0040	0.0070	0.0005	0.0036	0.0041	192	hours
0.0084	0.0044	0.0040	0.0045	0.0025	0.0056	264	hours
0.0104	0.0020	0.0050	0.0059	0.0080	0.0045	312	hours
0.0091	0.0075	0.0050	0.0050	0.0051	0.0041	360	hours
0.0114	0.0074	0.0069	0.0044	0.0074	0.0064	432	hours
0.0096	0.0061	0.0066	0.0045	0.0052	0.0057	480	hours
0.0076	0.0086	0.0075	0.0046	0.0067	0.0041	528	hours
0.0065	0.0096	0.0091	0.0045	0.0031	0.0072	600	hours
0.0086	0.0096	0.0005	0.0081	0.0072	0.0060	648	hours
0.0111	0.0096	0.0070	0.0040	0.0046	0.0056	696	hours
0.0070	0.0125	0.0091	0.0056	-0.0193	0.0041	768	hours
0.0121	0.0076	0.0071	0.0060	0.0057	0.0072	816	hours
0.0106	0.0096	0.0110	0.0060	0.0051	0.0051	864	hours

Appendix E

Raw data: absorptance

Measurement 1-10

										exposure time [h]
94.7	94.4	94.5	94.6	94.7	94.7	94.4	94.1	94.3	94.6	0
94.6	94.7	94.2	94.3	94.3	94.4	94.3	94.4	94.5	94.0	96
94.4	94.5	94.4	94.2	94.3	94.0	94.4	94.4	94.4	94.4	144
94.3	94.0	94.4	94.4	94.3	94.2	94.4	93.9	94.3	94.7	192
94.5	94.3	94.3	94.2	94.1	94.1	94.1	94.6	94.1	94.3	264
94.4	94.3	94.2	94.2	94.3	94.3	94.3	94.2	94.5	93.9	312
94.5	94.4	94.1	94.3	94.2	94.4	94.2	94.1	94.3	94.6	360
94.4	94.3	94.2	94.3	94.2	94.2	94.1	94.1	94.1	94.2	432
94.4	94.4	94.2	94.3	94.6	94.2	94.1	94.4	94.1	94.5	480
94.3	94.2	94.5	94.3	94.1	94.2	94.5	94.5	94.6	94.1	528
93.9	94.2	94.3	94.6	94.1	94.0	94.3	94.4	94.1	94.1	600
94.2	94.3	94.1	94.4	94.4	94.3	94.2	94.5	94.4	94.4	648
94.7	94.4	94.5	94.5	94.0	94.1	94.1	94.2	94.2	94.1	696
94.1	94.4	94.1	94.1	94.6	94.5	93.8	94.2	94.2	94.3	768
93.7	94.3	94.3	94.3	94.2	94.5	94.2	94.1	94.3	94.3	816
94.1	94.1	94.1	94.0	94.1	94.1	94.3	94.1	94.0	94.3	864

Measurement 11-20

94.7	95.6	94.5	94.5	94.9	94.8	95.0	94.9	94.9	94.6	0
94.9	95.0	94.7	95.8	94.9	94.7	94.5	94.7	94.7	94.7	96
94.8	94.5	94.6	94.3	94.9	94.4	94.4	94.4	94.4	94.9	144
94.7	94.9	94.6	94.5	94.4	94.9	94.6	94.5	94.6	94.8	192
94.8	94.6	94.6	94.5	94.7	94.7	94.7	94.7	94.5	94.6	264
94.9	94.6	94.7	94.8	94.7	94.7	94.7	94.4	94.5	94.7	312
94.8	94.1	94.7	94.6	94.4	94.6	94.6	94.7	94.7	95.2	360
94.8	94.6	94.4	94.6	94.5	94.3	94.5	94.2	94.7	94.3	432
95.1	94.9	94.8	94.8	94.2	94.5	94.8	94.6	94.8	94.8	480
94.3	94.6	94.7	94.6	94.5	94.3	94.7	95.1	94.7	94.6	528
94.7	94.6	94.4	94.3	94.8	94.2	94.5	94.4	94.5	94.2	600
94.7	94.5	94.6	94.5	94.0	94.7	94.5	94.7	94.5	94.4	648
94.5	94.6	94.3	94.5	94.7	94.8	94.9	94.4	94.5	94.6	696
94.8	94.6	94.7	94.6	94.7	94.7	94.3	94.2	94.7	94.3	768
94.7	94.7	95.0	94.7	94.4	94.4	94.7	94.3	94.3	94.5	816
94.6	94.5	94.6	95.0	94.2	94.6	94.6	94.6	94.2	94.3	864